國立臺灣大學理學院物理學研究所

碩士論文

Department of Physics

College of Science

National Taiwan University

Master Thesis

固定原子與傳輸原子量子位元的雙量子位元糾纏閘

Bypass entangling gate between a stationary and a flying neutral atom qubits

吳鈞季

Chun-Chi Wu

指導教授：林俊達 博士

Advisor: Guin-Dar Lin, Ph.D.

中華民國 111 年 7 月

July 2022

doi:10.6342/NTU202201550

doi:10.6342/NTU202201550

國立臺灣大學碩士學位論文
口試委員會審定書

固定原子與傳輸原子量子位元的雙量子位元糾纏閘
Bypass entangling gate between a stationary and a flying neutral atom qubits

本論文係吳鈞季君（R09222029）在國立臺灣大學物理學所完成之碩士學位論文，於民國 111 年 6 月 21 日承下列考試委員審查通過及口試及格，特此證明

口試委員：

林俊達（簽名）

（指導教授）

Ming-Shien Chang	Hsiang-Hua Jen

doi:10.6342/NTU202201550

doi:10.6342/NTU202201550

Acknowledgments

Since I joined Professor Lin's lab, I have met and gotten help from many wonderful people. It is my pleasure to acknowledge and cooperate with them. I want to thank them for enriching my life. First of all, I really appreciate my colleagues, ChenYu, Wenhan, Kuan-Ting, Hsu-Ting, Yu-Chen, and Yi-Lin giving me helpful advice for my research. Especillay, I want to thank Chen-Yu for helping me step into the AMO area since I was an inexperienced undergraduate student and Wenhan for being an incredible comrade when we dug into ion-trap-related research papers and quantum computing research. Secondly, I would like to thank my family for providing me with financial and mental support in pursuing this Master's degree. Your support undoubtedly gives me courage in these research years. Last but not least, I would like to thank my advisor, Professor Guin-Dar Lin, for patiently guiding my research work. Your invaluable advice not only gives me directions when I get stuck in research but also sheds light on the thinking of a theoretical physicist for me. I want to thank you for your advice somehow made me think like a theoretical physicist, and for your support without a second thought when I applied for Ph.D. It is my honor to work with you.

doi:10.6342/NTU202201550

doi:10.6342/NTU202201550

摘要

中性原子是易於發展可擴展的量子訊息處理平台的物理系統之一。本論文主要提出一個新穎的方案:用於量子訊息處理系統的原子被由一維光學晶格(optical lattice)和拉蓋爾-高斯光束 (Laguerre-Gaussian beam)組成的光阱 (optical trap)傳輸。此研究成果展示了在中性原子平台的量子訊息處理系統實現連結性(connectivity)的潛能。我們首先研究此新穎光阱的性質，並展示雙量子位元糾纏閘 （two-qubit entangling gate）作用於一顆靜止的原子和另一顆被此傳輸的原子(被稱爲Drive-Through方法)。在雙量子位元糾纏閘中，其中一顆移動的原子被藍頻失諧 (blue-detuned)一維光學晶格和拉蓋爾-高斯光束捕捉和傳輸，另一顆靜止的原子僅被光鑷捕捉。此Drive-Through方法被應用於兩個雙量子位元糾纏方案：雷德堡阻礙 （Rydberg blockade）方案和全耦合 （global coupling）方案。 當原子溫度達到 10 微開爾文 (microkelvin)時，兩種方案的保眞度階分別可以達到 0.99 和 0.999. 主要的誤差來源如原子溫度，都卜勒效應 (Doppler effect)和雷射強度誤差也在此論文中被分析。本論文亦研究策畫移動原子的行徑以避免加熱原子。伴隨著適當的傳輸軌跡，此過程僅激發少於10^{-3}個聲子 (phonon)。

中文關鍵字: 擴充的架構, 量子電腦, 雷德堡原子, 原子傳輸

doi:10.6342/NTU202201550

doi:10.6342/NTU202201550

Abstract

In this work, we theoretically investigate a novel scheme of quantum information processing via atom transportation. The scheme is based on a one-dimensional blue-detuned optical lattice and a blue-detuned Laguerre-Gaussian beam. We first studied the property of the relevant optical trap architecture. The implementation of two-qubit entangling gates on one stationary atom and one flying atom transported by a moving optical lattice, called as Drive-Through (DT) method, is also demonstrated. The DT method is implemented with two two-qubit entangling gate schemes, the Rydberg blockade scheme and the global coupling scheme, with gate fidelity>0.99 and >0.999, respectively, when the atomic temperature is about 10 μK . Error sources like finite temperature, the Doppler effect, and laser intensity deviation are analyzed. Movement manipulation of the flying atom to avoid heating while accelerating is also studied. After atomic movement are optimized, $< 10^{-3}$ phonons are excited. **Keywords: scalable architecture, quantum computer, Rydebrg atoms, atom transport**

doi:10.6342/NTU202201550

doi:10.6342/NTU202201550

Contents

doi:10.6342/NTU202201550

doi:10.6342/NTU202201550

doi:10.6342/NTU202201550

doi:10.6342/NTU202201550

List of Figures

doi:10.6342/NTU202201550

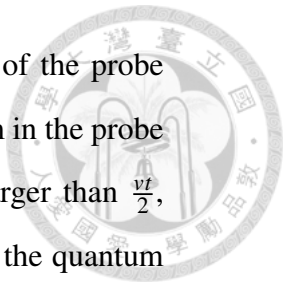

doi:10.6342/NTU202201550

doi:10.6342/NTU202201550

doi:10.6342/NTU202201550

List of Tables

doi:10.6342/NTU202201550

doi:10.6342/NTU202201550

Chapter 1

Introduction

Neutral atoms are promising systems for quantum information processing (QIP) [3, 4] given their potential for scalability. Besides, unlike superconducting qubits, each neutral atoms are inherently identical, so there are no defects in neutral atomic QIP system. The long coherence time for qubit encoded in atomic hyperfine states is also ideal for QIP.

With optical trapping techniques including optical lattices and tweezers [5, 6, 7], hundreds of qubits encoded in atoms were confined in optical trap arrays, and the physical system can be extended easily. The advantage in scalability makes neutral atoms an appealing physical platform for QIP and accordingly has been extensively studied in quantum simulation [8, 9, 10] and quantum computation [11, 12, 13, 14]. For recent research in QIP with neutral atomic systems, strong interactions [15, 16] between Rydberg atoms are often utilized to achieve high-fidelity multi-qubit gates [11, 13] and spin dynamics quantum simulations [9, 10].

Connectivity is inherently limited in neutral atomic systems, as neutral atomic arrays extend, the interaction range of Rydberg atoms is limited [17, 18] to their neighboring atoms. A pair of atoms far away from each other can not directly interact. To achieve connectivity in neutral atomic QIP systems, developments in long-range Rydberg-mediated QIP have been studied extensively, such as Rydberg-mediated interactions via photons [19, 20]and quantum state transport via atoms [21, 22]. Atom transportation via optical tweezers [23] also demonstrates the potential of long-range QIP. Yet, each scheme mentioned above has

doi:10.6342/NTU202201550

its own drawbacks. Photon-related gate schemes are of low efficiency and low fidelity. Quantum state transport schemes usually work with a complex setup and long operating time, which is experimentally impractical. As for qubits transport, the heating generated in transportation makes it hardly sustain repeated operations.

In this thesis, a new method is proposed to connect atoms based on a mediating qubit moving in acostnat motion. We aim to achieve qubit transport in QIP and avoid heating from the process. Unlike most recent works where neutral atoms were confined in stationary red-detuned optical tweezers or blue-detuned bottle beam trap arrays [6, 24], in this method, neutral atoms are trapped and transported by a potential well made of a blue-detuned optical lattice and a blue-detuned Laguerre-Gaussian beam. Meanwhile, no heating from the transport are generated when atoms are transferred with constant motion via controlling the optical lattice. Therefore, qubits are robust against the heating and motional effects during the long-range atomic transport. Besides, entanglement in one moving atom and the other stationary atom can be generated following a two-qubit entangling gate implementation. With the DT method, the Rydberg blockade scheme [16] and the global coupling scheme [11] with fidelity > 99% can be achieved, as current theoretical works in two-qubit gates via Rydberg interactions. Our study shows the potential to achieve arbitrary connectivity in trapped neutral atoms. DT method may also find further applications in other QIP.

The thesis is organized as follows: in the remaining of this chapter, we introduce atomic qubits, physical properties of Rydberg atoms, and optical traps for neutral atoms. We can see how the novel optical traps are constructed with these characteristics. In the end of this chapter, we will point out the motivation, and the aim of our works. In Chapter.2, the interaction between atoms and schemes for quantum computing via Rydberg atoms are presented. In Chapter.3, we introduce the blue-detuned interference Gaussian beam and Laguerre-Gaussian blue-detuned optical tweezers used to trap neutral atoms, and the properties of the optical traps are demonstrated. In Chapter.3 , the numerical results of the quantum gate with the DT method in the Rydberg blockade scheme and the global coupling scheme are demonstrated. The fidelity and error analysis for error sources, like

doi:10.6342/NTU202201550

atomic position fluctuation, Doppler effect, spontaneous emission, and errors from laser power are also analyzed. In Chapter.4, the heating effect from acceleration is discussed. Engineering the process to prevent heating is also demonstrated. In the end, the conclusion is given in Chapter.5.

1.1 Atomic qubits

For neutral atom QIP, a qubit is encoded into two internal states. When the qubit is in a pure state, it can be represented by a superposition of these two internal states $|\psi\rangle = cos\frac{\theta}{2}|g\rangle + e^{i\phi}|e\rangle$. The Hamiltonian of a neutral atom can be written as

$$H_{atom} = \frac{\hbar\omega}{2}(|e\rangle\langle e| - |g\rangle\langle g|) \tag{1.1.1}$$

where $\{|e\rangle, |g\rangle\}$denotes the qubit states, ω denotes the dipole transition frequency between two states. θ and ϕ represent the polar angle and the azimuthal angle of the state vector in the Bloch sphere. Most of the experiment works on neutral atomic QIP systems use heavy alkali atoms, like Rb and Cs, which can be cooled and trapped readily. For QIP, the internal states with high coherence time and high lifetime are preferable for encoding qubits, so qubits are usually encoded in hyperfine or Zeeman ground states for their long coherence [4]. Another advantage of encoding qubits in hyperfine manifolds is that the transition frequency is in gigahertz orders. Therefore, high fidelity control on qubits can be implemented via microwaves [25]. In recent quantum computing experiments, qubits are encoded in the clock states due to their insensitivity to magnetic field fluctuations. For qubits encoded in fine structure and hyperfine structure manifolds, a monochromatic laser can not couple atomic states directly. However, these states can still be coupled in a two-photon transition via a metastable state, also known as stimulated Raman transition.

doi:10.6342/NTU202201550

1.2 Rydberg atom

In this section, we introduce the basic properties of a Rydberg atom, including lifetime, size, and sensitivity to external fields. The interaction between Rydberg atoms is left in Sec.2.1.

Rydberg atoms are atoms with highly excited electronic states with the principal quantum number of these states $n \gg 1$. The Physical properties of Rydberg states are mainly determined by the principal quantum number n. The lifetime of low angular momentum Rydberg states is determined by spontaneous electric dipole transitions and blackbody radiation [26]. For finite temperatures, the lifetime τ_{nl} of a Rydberg-state with principal quantum number n and angular momentum number l follows the relationship

$$\frac{1}{\tau_{nl}} = \frac{1}{\tau_{nl}^{(0)}} + \frac{1}{\tau_{nl}^{(bb)}} \tag{1.2.1}$$

where $\tau_{nl}^{(0)}$ denotes the zero-temperature lifetime, and $\tau_{nl}^{(bb)}$ denotes the blackbody radiation lifetime. $\tau_{nl}^{(0)}$ is determined by all allowable electric dipole transitions and can be represented as

$$\frac{1}{\tau_{nl}^{(0)}} = \sum_{n',l'} A_{nl\to n'l'} \tag{1.2.2}$$

where A is the Einstein-A coefficient. $\tau_{nl}^{(0)}$ is roughly proportional to n^3 for the alkali atoms.

As for the blackbody radiation lifetime $\tau_{nl}^{(bb)}$, it can be estimated as

$$\tau_{nl}^{(bb)} = \frac{4\alpha^3 k_B T}{3\hbar n^2} \tag{1.2.3}$$

where α denotes the fine structure constant, k_B denotes the Boltzmann constant, $\hbar$ denotes the Planck constant, and T represents the temperature of the atom.

The typical lifetimes of Rydberg states of Cs are shown in Fig.1.1. (The figure is simulated with the extended package, Alkali.ne Rydberg Calculator.) Typically, the lifetime of

doi:10.6342/NTU202201550

room-temperature Rydberg atoms for low angular momentum with $n \approx 50$ is over 50 μs . As for the typical lifetimes of Rydberg states of Rb, see Saffman's work [1].

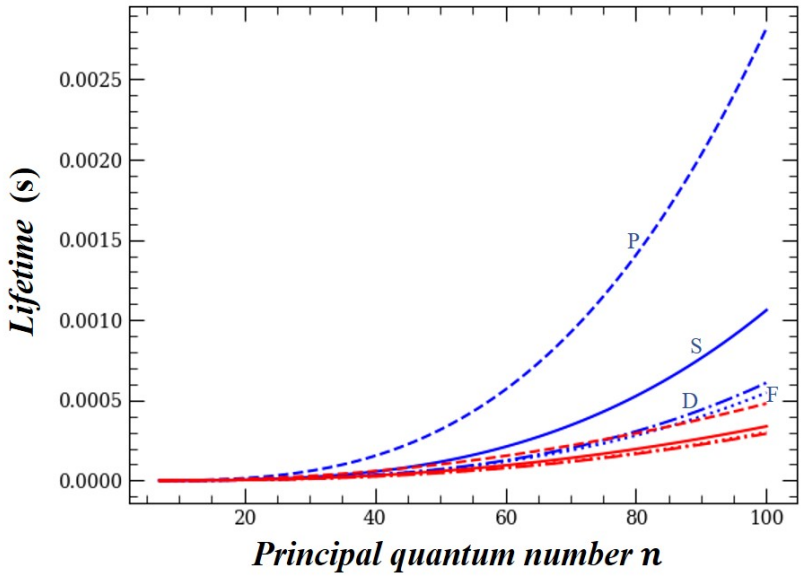

Figure 1.1: Excited-state lifetime due to radiative decay of S, P, D and F states of Cs for T = 0 K (blue lines) and T = 300 K (red lines) [1].

The relationship between the principal quantum number n and the size of Rydberg atoms can be estimated by the Bohr model. For alkali atoms, the atoms can be viewed as effective single-electron atoms. Therefore, the radius of the Rydberg atom can be estimated as

$$r_n \approx \frac{n^2\hbar^2}{Zk_e e^2 m_e} \tag{1.2.4}$$

where Z denotes the atomic number, k_e denotes the Coulomb constant, e is the electric charge, and m_e represents the electric mass. The radius of Rydberg-state atoms is roughly proportional to n^2.

A Rydberg-state atom is extremely sensitive to the external field due to its large electronic dipole. When Rydberg atoms are in low-intenisty electric fields, the corresponding energy shift can be estimated by a perturbation theory. Take dc electric field as an example, the

doi:10.6342/NTU202201550

first non-zero Stark shift from the field

$$\Delta E \backsim \frac{(eE)^2\langle r\rangle^2}{E_{tran}} \backsim \frac{n^7\hbar^6E^2}{Z^4k_e^4e^6m_e^3}. \tag{1.2.5}$$

Where ΔE denotes the Stark shift, E is the amplitude of the dc field, and E_{tran} is transition energy between states. The sensitivity to the electric field limits Rydberg states with excessively high n for QIP experiments. The environmental electric field should be well controlled to avoid energy fluctuations.

1.3 Mechanism of optical traps and laser beams

In previous sections, we have shown a neutral atom qubit encoded in its internal states, and the physical properties of a Rydberg atom. In this section, we will see how to trap a neutral atom via lasers.

1.3.1 Optical tweezers and gradient force

Optical tweezers are highly focused laser beams capable of trapping and manipulating dielectric particles in nanometer-sized. When nanometer-scaled dielectric particles like neutral atoms are in the electric field, these particles can be viewed as point dipoles that interact with the electric field. As in the inhomogenous electric field, these particles feel the gradient force from the dipole potential gradient. The force direction is determined by the sign of the polarizability of particles. If a particle with negative (positive) polarizability under the electric field, the particle will be repelled (attracted) to the place with lower (higher) field intensity. This is the essential mechanism for dipole traps, including optical tweezers and lattices.

Neutral atoms are often trapped by red-detuned or blue-detuned optical dipole traps. For red-detuned dipole traps, optical tweezers are composed of focused Gaussian beams. The beam waist of optical tweezers contains a strong electric field gradient. Atoms will be

doi:10.6342/NTU202201550

trapped in the area with a stronger electric field due to the positive polarizability. On the other hand, blue-detuned dipole traps are geometrical hollow, like doughnut-shaped and bottle-shaped beams. With negative polarizability, atoms will be repelled to the trap center, the area with relatively low field intensity.

1.3.2 Ponderomotive potential

When a charged particle is in an inhomogeneous oscillating electromagnetic field, the particle will move towards the area with low field strength. Take a negative charge particle as an example. The motion of this particle can be divided into two half-period of oscillations. In the first half period, the particle feels the electromagnetic field and tends to move towards an area with stronger field strength. In the second half-period, the particle moves in the opposite direction due to the opposite field strength sign in the second half period. However, the particle is at the place with a stronger field strength in the second half period. Therefore, the net impulse the particle received in a whole period will push the particle towards the area with weaker field strength. The time-averaged ponderomotive potential of a charged particle is

$$U(\overrightarrow{r}) = \frac{e^2}{2\epsilon_0 cm\omega^2} I(\overrightarrow{r}) \tag{1.3.1}$$

where ϵ_0 is the vacuum permittivity, m is the mass of the particle, ω is the field oscillation frequency, $I(\overrightarrow{r})$ is the laser amplitude at position $\overrightarrow{r}$.

For an alkali Rydberg atom, the valence electron is far from the atomic nucleus and other electrons. Therefore, the valence electron will experience ponderomotive force as a free electron in an oscillating electromagnetic field. Meanwhile, the atomic nucleus and other electrons can be viewed as a positive charge particle. However, the ponderomotive potential of a Rydberg atom is almost the same as the potential of a free electron due to the large nucleus-to-electron mass ratio. The ponderomotive potential of a nucleus can be neglected. In other words, a heavy particle has larger inertia, so it is harder to swing with the oscillating electromagnetic field. The acceleration a is proportional to m^{-1}. There-

doi:10.6342/NTU202201550

fore, the oscillation length of a particle is also proportional to m^{-1}. The corresponding ponderomotive potential is propotional to $m\times(\text{oscillation length})^2 \sim m^{-1}$.

1.3.3 Lauguerre-Gaussian beam

When the laser beam profile is circularly symmetric, the laser beam can be decomposed into Laguerre-Gaussian modes. These modes can be performed by generalized Laguerre polynomials in cylindrical coordinates. The amplitude of the Laguerre-Gaussian mode

$$u_{lp}(r,\phi,z) = \sqrt{\frac{2p!}{\pi(p+|l|)!}}(\frac{-2r^2}{w^2(z)})^{|l|/2}(L_p^{|l|}(\frac{2r^2}{w^2(z)}))e^{\frac{-r^2}{w^2(z)}}e^{(-i\frac{kr^2z}{2(z^2+z_R^2)}-il\phi+i(2p+l+1)tan^{-1}(\frac{z}{z_R}))} \tag{1.3.2}$$

where $w(z)$ is the beam width, k is the wavevector, z_R is the Rayleigh range, and $L_p^{|l|}$ is are the generalized Laguerre polynomials with mode index $l$and p. r,ϕ,z are the position represented in cylindrical coordinates. In an atomic experiment, Laguerre-Gaussian beam with mode index $l=1,p=0$ are often used to trap neutral atoms due to its doughnut-shaped intensity distribution. With a blue-detuned laser, ground-state atoms and Rydberg-state atoms can be trapped inside the beam center, the area with near null laser intensity, via gradient force and ponderomotive force respectively.

1.4 Motivation

Experimental results show the possibility of realizing QIP in neutral atom systems. However, there are still other issues needed to be addressed. One of the issues is that the interaction range for atoms is limited. Therefore, two-qubit gates cannot be implemented directly on two distant atoms. Current schemes in connecting neutral atoms are still deficient. Based on the concept of qubit transport, our proposal aims to avoid heating while achieving connectivity on an atomic system. In the Drive-Through method, an entangling gate is implemented on one stationary atom and the other flying qubit shuttled by an opti-

doi:10.6342/NTU202201550

cal lattice. The optical lattice is served as the carrier for long-distance atom transportation. However, as atom transportation via optical tweezers [23], heating and atomic loss may occur when the flying qubit is shuffled by an optical lattice. The number of repeated operations are also limited by unwanted heating. Besides, cooling of qubit atoms is prohibited during QIP since the information encoded in qubits will be ruined by atomic cooling. A way out of the dilemma is designing the atomic movement path [27] to avoid unnecessary heating and atomic loss in transport. In our work, the flying qubit can move along with the optical lattice without stopping during the entangling process. By doing so, less heating can be expected. Therefore, two distant atoms can be connected physically, providing a possibility of arbitrary connectivity in neutral atom systems and avoiding heating during qubit transport. One can further diminish the heating by engineering the movement of the flying qubit.

doi:10.6342/NTU202201550

doi:10.6342/NTU202201550

Chapter 2

Quantum computation with neutral atoms

In the previous section, we have presented the basic properties of Rydberg atoms and optical traps used to confine atoms, and they can be incorporated into the design of neutral atom QIP systems. Yet, to implement a two-qubit entangling gate on an atomic system, the interaction between atoms should be precisely utilized and manipulated. In this section, we will introduce the interaction between atoms. The Rydberg blockade scheme and the global coupling scheme, two-qubit entangling gate schemes based on the strong interaction, are also presented. At the end of this chapter, we will review current experimental progresses, diagnose the weakness in these schemes.

2.1 Interaction between atoms

In this section, we will introduce the interaction between two atoms, including dipole-dipole interaction and van der Waals interaction. The strong interaction between Rydberg atoms is the key mechanism for two-qubit entanglement.

doi:10.6342/NTU202201550

2.1.1 Dipole-dipole inteaction

With intrinsic large dipole moments, Rydberg atoms interact with each other strongly via dipole-dipole interaction. The dipole-dipole interaction between Rydberg atoms has been extensively studied for QIP. The dipole interaction operator

$$\hat{V} = \frac{1}{4\pi\epsilon_o R^3}(\hat{\mathbf{d}_1}\cdot\hat{\mathbf{d}}_2 - 3(\hat{\mathbf{d}}_1\cdot\hat{\mathbf{r}})(\hat{\mathbf{d}_2}\cdot\hat{\mathbf{r}})) \tag{2.1.1}$$

where R is the distance between two atoms, $\hat{\mathbf{r}}$ is the unit vector connecting two atoms, and $\hat{\mathbf{d}_1}$ and $\hat{\mathbf{d}_2}$ are the dipole operator of each atom. The corresponding Hilbert space is spanned by a two-atom internal state basis.

Dipole-dipole interaction stems from virtual photons exchanges between atoms. For example, in a two level-system encoded in basis $\{|e\rangle, |g\rangle\}$, the first atom is in the excited state $|e\rangle$, and the second atom is in the ground state $|g\rangle$. The first atom can emit a photon and decay to the ground state. Meanwhile, the second atom absorbs this photon and excites it to the excited state. The interaction results in the state exchange between two atoms, or energy shift in a collective basis.

2.1.2 Van der Waals interaction

When two atoms are in the same states, the first-order dipole-dipole interaction is usually not dominated because of the large energy defect. However, the second-order dipole-dipole interaction can still be strong. For example, a pair of atoms in state $|\alpha\rangle$ is considered. The first atom can emit a photon and decay to $|\beta\rangle$, while the second atom absorbs this photon and excites to another state $|\gamma\rangle$. An energy defect $\delta_E = E_\beta + E_\gamma - 2E_\alpha$ from the process will suppress the occurrence of this process. However, if the time is short and the coupling strength is strong enough, the virtual photon can exchange again from the

doi:10.6342/NTU202201550

virtual state $|\beta\rangle|\gamma\rangle$, and the atomic state returns to $|\alpha\alpha\rangle$. The interaction strength is

$$C_{\alpha\alpha} = \sum_{|i,j\rangle} \frac{\langle\alpha\alpha|\hat{V}|i,j\rangle\langle i,j|\hat{V}|\alpha\alpha\rangle}{2E_1 - E_i - E_j} = \frac{C_{6,\alpha\alpha}}{R^6} \tag{2.1.2}$$

where $|i,j\rangle$ is the allowable virtual pair-state. $C_{6,\alpha\alpha}$ is the van der Waals coefficient.

Another explanation of van der Waals interaction is the perturbation of dipole-dipole interaction. The first-order dipole-dipole interaction of the atomic state $|\alpha\alpha\rangle$ is zero due to parity. Therefore, the interaction energy determines by the second-order perturbation.

The energy shift from van der Waals interacion mainly depends on the principal quantum number and interatomic distance. When only the strongest-coupling virtual state is considered, $\frac{C_{6,\alpha\alpha}}{R^6} \sim \frac{|\mathbf{d}|^4}{R^6(\Delta E)} \sim \frac{n^8}{R^6 n^{-3}} \sim \frac{n^{11}}{R^6}$. In reality, many virtual states may contribute to the same order of magnitude. Also, the interaction strength may be tuned by applying an external field intentionally (Sec. 1.2). Via tuning energy defects, the van der Waals interaction strength may also be engineered for QIP.

When the orientation of two atoms are parallel to quantization axis of the atoms, the Rydberg interaction strength [2], $H_{vdw}|\varphi\rangle = \frac{C_6}{R^6} D|\varphi\rangle = \frac{C_6}{R^6} D_\varphi|\varphi\rangle$, where $H_{vdw} = \sum_{|i,j\rangle} \frac{\hat{V}|i,j\rangle\langle i,j|\hat{V}}{-\delta_{ij}}$, δ_{ij} is the Förster defect with respect to the initial state. The interaction strength can be decomposed of radial and angular momentum components. C_6 only depends on the atomic energy level and radial matrix elements, the operator D determines all the angular momentum properties, and $D_\varphi$is the eigenvalue of D. For atomic orbital momentum is in s state, the value of D_φ is in the table.

Channel	$\|M\|$	$\{D_\varphi\}$
$s_{1/2}+s_{1/2} \rightarrow p+p$	1	$\{1.33\}$
$s_{1/2}+s_{1/2} \rightarrow p+p$	0	$\{1.33, 1.33\}$
$s_{1/2}+s_{1/2} \rightarrow p_{1/2}+p_{1/2}$	1	$\{0.0988\}$
$s_{1/2}+s_{1/2} \rightarrow p_{1/2}+p_{1/2}$	0	$\{0.395, 0\}$
$s_{1/2}+s_{1/2} \rightarrow p_{1/2}+p_{3/2}$	1	$\{0.346\}$
$s_{1/2}+s_{1/2} \rightarrow p_{1/2}+p_{3/2}$	0	$\{0.444, 0.0494\}$
$s_{1/2}+s_{1/2} \rightarrow p_{3/2}+p_{3/2}$	1	$\{0.543\}$
$s_{1/2}+s_{1/2} \rightarrow p_{3/2}+p_{3/2}$	0	$\{0.844, 0.444\}$

Table 2.1: The table of D_φ for s-state atoms. $|M|$ is the absolute value of the angular momentum sum. [2]

doi:10.6342/NTU202201550

In this thesis, Alkali.ne Rydberg Calculator is used for van der Waals interaction strength calculation. For atoms in $|100S_{1/2}, m_s = 1/2\rangle$, the van der Waals interaction strength is

$$\frac{1}{R^6}\Sigma_{n',n''}(0.0988 \times C_{6,|100S_{1/2}\rangle,|100S_{1/2}\rangle,|n'P_{1/2}\rangle,|n''P_{1/2}\rangle} + 2 \times 0.346 \times C_{6,|100S_{1/2}\rangle,|100S_{1/2}\rangle,|n'P_{1/2}\rangle,|n''P_{3/2}\rangle} + 0.543 \times C_{6,|100S_{1/2}\rangle,|100S_{1/2}\rangle,|n'P_{3/2}\rangle,|n''P_{3/2}\rangle})$$

where $C_{6,|\alpha\rangle|\alpha\rangle,|\beta\rangle,|\gamma\rangle}$ is the C_6 value for channel $|\alpha\rangle|\alpha\rangle$ to $|\beta\rangle|\gamma\rangle$.

The atomic interaction strength is also determined by the relative orientation of two atoms. As in Fig. 2.1, atomic interaction strength varies with the relative polar angle and the azimuthal angle. In the DT-method, the polar angle θ changes as the flying qubit moves. The interaction strength is $2\pi \times 44.32$ MHz when the distance between atoms is 10 μm and the polar angle is 0. The interaction strength varies as the distance and the relative polar angle change when the flying atom moves.

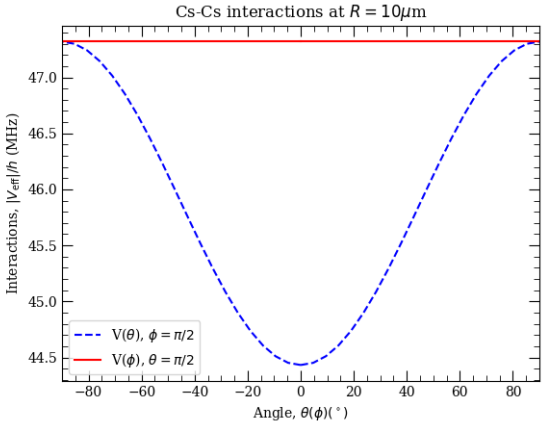

Figure 2.1: Rydberg interaction between different angles

2.1.3 Rydberg blockade

Large van der Waals interaction between Rydberg atoms greatly alters the atomic state dynamics. If a Rydberg atom already exists, other neighboring atoms can not be excited to the Rydberg state even though a resonant laser probes on the Rydberg transition of

doi:10.6342/NTU202201550

neighboring atoms. It is because the Rydberg state energy of neighboring atoms is shifted by the strong interaction when another Rydberg atom already exists. The range for the Rydberg blockade, called the blockade radius R_b, is defined as

$$\frac{C_{6,\alpha\alpha}}{R_b^6} = \frac{\gamma}{2} \tag{2.1.3}$$

where γ denotes the linewidth excitation.

We then have

$$R_b = (\frac{2C_{6,\alpha\alpha}}{\gamma})^{1/6} \tag{2.1.4}$$

2.2 Quantum computing with Rydberg atoms

In this section, we will demonstrate how the Rydberg blockade is used for implementing QIP. In quantum computing, every operation on qubits can be described as a quantum circuit. In this model, a quantum logic gate is a basic unit operating on qubits, also a block for building up the whole quantum circuit. Each quantum logic gate can be decomposed into a sequence of universal quantum gates. Usually, a set of universal quantum gates can be constructed by rotation operators, the phase shift gate, and the CNOT gate (or controlled phase-flip gate). Therefore, these quantum gates should achieve high fidelity to realize quantum computing on a physical system. For neutral atomic systems, single-qubit gates, like rotation operators and the phase shift gate, can be implemented via precise laser control and achieve high fidelity for QIP. Therefore, we mainly focus on a two-qubit entangling gate in the following sections.

2.2.1 Rydberg blockade scheme

Rydberg blockade (Sec.2.1.3.) can be used for constructing a controlled phase-flip gate. When a Rydberg atom already exists, the transition to the Rydberg state is limited for neighboring atoms due to large energy shift by strong Rydberg coupling. Therefore, if

doi:10.6342/NTU202201550

the controlled qubit is excited to the Rydberg state, excitation to the Rydberg state will be blockaded on the target qubit, and a non-trivial 2π-pulse rotation will be hampered.

Qubits in basis $\{|0\rangle, |1\rangle\}$ are used as an example. We assume that only atoms in $|1\rangle$ interact with laser and can be excited to the Rydberg state $|r\rangle$. The scheme is as follows: Firstly, a π-pulse on controlled qubit is implemented. Then, a 2π-pulse on the target qubit is implemented. In the end, an additional π-pulse on the controlled qubit is implemented to drive the controlled qubit back to its initial state [16]. (Fig.2.2.)

The Hamiltonian of each pulse is

$$H_c = e^{i(kx_c - v_c t)}\Omega|r\rangle_c\langle 1| + V|rr\rangle\langle rr| + h.c. \tag{2.2.1}$$

$$H_t = e^{i(kx_t - v_t t)}\Omega|r\rangle_t\langle 1| + V|rr\rangle\langle rr| + h.c. \tag{2.2.2}$$

$$H_c = e^{i(kx_c - v_c t)}\Omega|r\rangle_c\langle 1| + V|rr\rangle\langle rr| + h.c. \tag{2.2.3}$$

where x_c (v_c), x_t (v_t) is the position (The Doppler frequency due to the relative velocity to the laser) of the controlled qubit and the target qubit, respectivel. V is the Rydberg interaction energy, and Ω is Rabi frequency between the ground state and the Rydberg state.

For each element in two-qubit basis $\{|0\rangle|0\rangle, |1\rangle|0\rangle, |0\rangle|1\rangle, |1\rangle|1\rangle\}$, the ideal evolution will be

$$|0\rangle_c|0\rangle_t \xrightarrow{U_c} |0\rangle_c|0\rangle_t \xrightarrow{U_t} |0\rangle_c|0\rangle_t \xrightarrow{U_c} |0\rangle_c|0\rangle_t \tag{2.2.4}$$

doi:10.6342/NTU202201550

$$|1\rangle_c|0\rangle_t \xrightarrow{U_c} i|r\rangle_c|0\rangle_t \xrightarrow{U_t} i|r\rangle_c|0\rangle_t \xrightarrow{U_c} -|1\rangle_c|0\rangle_t \tag{2.2.5}$$

$$|0\rangle_c|1\rangle_t \xrightarrow{U_c} |0\rangle_c|1\rangle_t \xrightarrow{U_t} -|0\rangle_c|1\rangle_t \xrightarrow{U_c} -|0\rangle_c|1\rangle_t \tag{2.2.6}$$

$$|1\rangle_c|1\rangle_t \xrightarrow{U_c} i|r\rangle_c|1\rangle_t \xrightarrow{U_t} i|r\rangle_c|1\rangle_t \xrightarrow{U_c} -|1\rangle_c|1\rangle_t \tag{2.2.7}$$

, where U_c, U_t represents a π pulse on the controlled qubit and a 2π pulse on the target qubit. With this scheme, an entangling gate is achieved. In two-qubit basis, the evolution operator

$$U = \begin{pmatrix} 1 & 0 & 0 & 0 \\ 0 & e^{i\pi} & 0 & 0 \\ 0 & 0 & e^{i\pi} & 0 \\ 0 & 0 & 0 & e^{i\pi} \end{pmatrix} \tag{2.2.8}$$

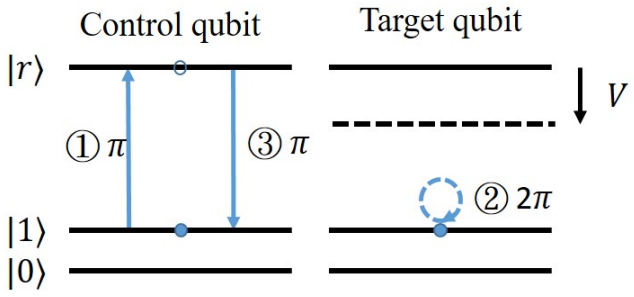

Figure 2.2: Rydberg blockade scheme

doi:10.6342/NTU202201550

2.2.2 Global coupling scheme

In this scheme, two atoms are probed by lasers simultaneously, and the collective state basis is considered during the evolution. Qubits with basis $\{|0\rangle, |1\rangle\}$ are used as an example. We assume that only atoms in state $|1\rangle$ interact with laser and can be excited to Rydberg state $|r\rangle$. Each qubit state evolves with different rotation paths on Bloch's sphere. For $|1\rangle|1\rangle$ coupled to the entangled state $|\Psi_+\rangle$, the Rabi frequency is higher by $\sqrt{2}$. Therefore, $|1\rangle|0\rangle$ and $|0\rangle|1\rangle$ evolve an incomplete rotation after the laser pulse. However, by applying a second laser pulse with a specific relative phase, $|1\rangle|0\rangle$ and $|0\rangle|1\rangle$ will return to their initial states [11] (Fig. 2.3). By choosing laser detuning, laser intensity, and relative phase between two pulses, an entangling phase gate can be achieved. Rydberg blockade is utilized implicitly to block the state excitation from the collective state to the double-excited Rydberg states.

The Hamiltonian of each pulse is

$$\begin{aligned} H_1 =& \Omega(e^{i(kx_1 - v_1 t)}|1\rangle|r\rangle + e^{i(kx_2 - v_2 t)}|r\rangle|1\rangle)\langle 1|\langle 1| - \Delta(|1\rangle|r\rangle + |r\rangle|1\rangle)\langle 1|\langle 1| \\ &+ (V - 2\Delta)|r\rangle|r\rangle\langle r|\langle r| + h.c. \end{aligned} \tag{2.2.9}$$

$$\begin{aligned} H_2 =& \Omega e^{i\xi}(e^{i(kx_1 - v_1 t)}|1\rangle|r\rangle + e^{i(kx_2 - v_2 t)}|r\rangle|1\rangle)\langle 1|\langle 1| - \Delta(|1\rangle|r\rangle + |r\rangle|1\rangle)\langle 1|\langle 1| \\ &+ (V - 2\Delta)|r\rangle|r\rangle\langle r|\langle r| + h.c. \end{aligned} \tag{2.2.10}$$

where x_1 (v_1), x_2 (v_2) is the position (The Doppler frequency due to the relative velocity to the laser) of the first qubit and the second qubit, respectively. V is the Rydberg interaction energy, $\Delta$is the laser detuning, ξ is the relative phase between two pulses, and Ω is Rabi frequency between the ground state and the Rydberg state.

For each element in two-qubit basis $\{|0\rangle|0\rangle, |1\rangle|0\rangle, |0\rangle|1\rangle, |1\rangle|1\rangle\}$, the ideal evolution will

doi:10.6342/NTU202201550

be:

$$|0\rangle|0\rangle \xrightarrow{U_1} |0\rangle|0\rangle \xrightarrow{U_2} |0\rangle|0\rangle \tag{2.2.11}$$

$$|0\rangle|1\rangle \xrightarrow{U_1} |\psi\rangle \xrightarrow{U_2} e^{i\phi_{01}}|0\rangle|1\rangle \tag{2.2.12}$$

$$|1\rangle|0\rangle \xrightarrow{U_1} |\psi'\rangle \xrightarrow{U_2} e^{i\phi_{10}}|1\rangle|0\rangle \tag{2.2.13}$$

$$|1\rangle|1\rangle \xrightarrow{U_1} e^{i\phi_{11}/2}|1\rangle|1\rangle \xrightarrow{U_2} e^{i\phi_{11}}|0\rangle|0\rangle \tag{2.2.14}$$

where U_1, U_2 represent the evolution operator of the first pulse and the second pulse, $|\psi\rangle$ ($|\psi'\rangle$) denotes the intermediate states of $|1\rangle|0\rangle$ ($|0\rangle|1\rangle$) after the first pulse, respectively.

In two-qubit basis, the evolution operator

$$U = \begin{pmatrix} 1 & 0 & 0 & 0 \\ 0 & e^{i\phi_{01}} & 0 & 0 \\ 0 & 0 & e^{i\phi_{10}} & 0 \\ 0 & 0 & 0 & e^{i\phi_{11}} \end{pmatrix} \tag{2.2.15}$$

With a phase shift gate on $|1\rangle$ and parameters resulting in $\phi_{11} - \phi_{01} - \phi_{10} = \pi$, an entangling gate is achieved. In this scheme, Rydberg blockade prevents $|1\rangle|1\rangle$ from exciting to the double-excited Rydberg state $|r\rangle|r\rangle$. $|1\rangle|1\rangle$ can only excite to the entangled state $|\Psi_+\rangle = \frac{1}{\sqrt{2}}(|1\rangle|r\rangle + |r\rangle|1\rangle)$ and return. However, even when the van der Waals interaction is not strong enough, the global coupling scheme can still work by tuning the parameters.

doi:10.6342/NTU202201550

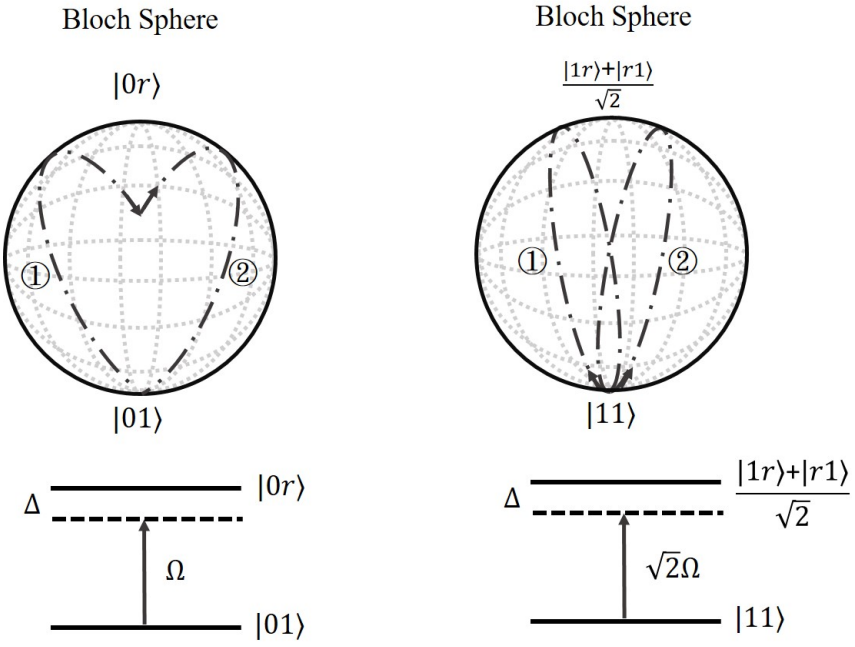

Figure 2.3: Global coupling scheme

2.3 Experimental progress in neutral atom quantum information processing

DiVincenzo's criteria are conditions necessary for building up a quantum computer. One of the conditions is to assure scalability with well-characterized qubits in a physical system. A single well-characterized qubit can be created and defined, but involving a large number of qubits in a system is still challenging. Another condition is long relevant decoherence times. The quantum information will be destroyed by natural decoherence. Thus, a long coherence time compared to the gate operation is necessary for a system. Also, to confront the intrinsic decoherence, a quantum error correction scheme should be able to work on the system, and a quantum gate should be implemented with fidelity better than 0.9999 to realize quantum error correction. For a neutral atomic system, there is a great potential to realize scalablity via optical lattices or tweezer arrays, and the qubit numbers are still progressing. As for high fidelity quantum gate issues in a neutral atom system, a single-qubit gate with fidelity better than 0.99 is achieved [28, 25], but a high fidelity two-qubit gate is still challenging. Therefore, a scalable atomic system and a higher fidelity two-qubit entangling gate are two of the main challenges for realizing QIP

doi:10.6342/NTU202201550

in neutral atom systems. To address these issues, significant experimental progress has been demonstrated in neutral atomic QIP systems.

In recent works, blue-detuned optical lattices [12] and red-detuned optical tweezer arrays [11] are used for building atomic arrays. The blue-detuned optical lattices are composed of a blue-detuned Gaussian beam array [29] or square grid of lines of light. Atoms are confined in each unit cell and construct an atomic array. In this work [12], an atomic qubit array with 121 sites are demonstrated with an average filling fraction of 55%. A red-detuned two-dimensional (2D) optical tweezer array is formed by a spatial light modulator [7]. Via dynamically moving optical tweezers, atoms can be moved and rearranged, and atomic arrays of up to hundreds of atoms with an average filling fraction exceeding 99%.

Recent experimental results in two-qubit entangling gates are still far from the quantum error correction criterion. In Saffman's work [12, 14], the Rydberg blockade scheme is used for implementing a two-qubit entangling gate with fidelity ≈ 0.92. In Lukin's work [11], the global coupling is used for implementing a two-qubit entangling gate, and fidelity > 0.97 is demonstrated. Many issues still limit the fidelity, like doppler dephasing, atomic position error, photon scattering, and spontaneous emission of Rydberg states. Yet, in theoretical calculations, fidelity better than 0.99 is still available.

doi:10.6342/NTU202201550

doi:10.6342/NTU202201550

Chapter 3

Two-qubit gate implementation with the drive-through method

In this chapter, we will introduce how to realize quantum gates in the DT method. One of the main issues of the DT method is the spatial confinement and transport of atoms. Another issue is the two-qubit gate implementation on moving qubits. To address the spatial confinement of atoms, blue-detuned optical traps for trapping atoms will be introduced first. We shall see how a blue-detuned optical lattice and a blue-detuned Laguerre-Gaussian beam can trap atoms in all conditions. As for the two-qubit gate implementation, the varied interaction strength between Rydberg-state atoms due to the change of the distance between atoms and relative orientation angle should be taken into account. The performance and the error analysis of the two-qubit gate implementation in the DT method will also be demonstrated in this chapter.

3.1 Blue-detuned optical traps

In the DT method, the optical traps are kept on to trap atoms during the quantum gate implementation. If the optical traps were off, atoms would be free during the quantum information processing and might be lost. Therefore, ground-state atoms and Rydberg-state atoms should both be confined in optical traps. Blue-detuned optical traps with specific

doi:10.6342/NTU202201550

wavelengths are ideal for atomic confinement since ground-state atoms and Rydberg-state atoms can be confined by dipole gradient force and ponderomotive force separately. With blue-detuned optical traps, atoms are trapped in the area with null laser intensity near trap centers.

3.1.1 Blue-detune one-dimensional optical lattice

Blue-detuned counter-propagating Gaussian beams are used for trapping atoms in the longitudinal direction. The trap potential of ground-state atoms is $U(\overrightarrow{r}) = \frac{-1}{2\epsilon_0 c}\alpha I(\vec{r})$, where α is the polarizability, and I is the intensity in position $\overrightarrow{r}$. For counter-propagating Gaussian beams, the intensity

$$\begin{aligned} I(\rho,z) &= \frac{2P_1}{\pi w_1^2}\Big|\frac{w_1}{w_1(z)}e^{-\frac{\rho^2}{w_1^2(z)}}e^{i[kz+k\frac{\rho^2}{2R_1(z)}-\eta_1(z)]} \\ &\quad -\frac{w_2}{w_2(z)}e^{-\frac{\rho^2}{w_2^2(z)}}e^{i[-kz+k\frac{\rho^2}{2R_2(z)}+\eta_2(z)]}\Big|^2 \end{aligned} \tag{3.1.1}$$

where P_1, P_2 are the power of the Gaussian beams respectively, and $w_1, w_2$are the beam waist of the Gaussian beams respectively. ρ and z are the distance from trap center in radial direction and longitudinal direction. $z_{R_{1,2}} = \frac{\pi w_{1,2}^2}{\lambda}$, where λ is the wavelength of the laser.$w_{1,2}(z) = w_{1,2}\sqrt{1+(\frac{z}{z_{R_{1,2}}})^2}$. $R_{1,2}(z) = z + \frac{z_{R_{1,2}}^2}{z}$.$\eta_{1,2}(z) = tan^{-1}(\frac{z}{z_{R_{1,2}}})$.$\rho^2 = x^2+y^2$.We also assume $\frac{P_1}{w_1^2} = \frac{P_2}{w_2^2}$.

For Rydberg-state atoms, the ponderomotive potential is dominated by the valence electron. However, the spatial distribution of the valence electrons is comparable to the size of the optical trap, so the optical trap intensity changing over space should be considered for the potential. The ponderomotive potential of the Rydberg-state atoms is [30, 31]

$$U(\overrightarrow{r}) = \frac{e^2}{2\epsilon_0 c m_e \omega^2}\int d^3r I(\overrightarrow{R}+\overrightarrow{r})|\psi^0(\overrightarrow{r};\overrightarrow{R})|^2 \tag{3.1.2}$$

where e and m_e are the electron charge and mass. c is the speed of light, ω is the frequency

doi:10.6342/NTU202201550

of the electric field.$\psi^0(\overrightarrow{r};\overrightarrow{R})$ is the wave function of the Rydberg-state electron for the Rydberg state atom in $\overrightarrow{R}$.

3.1.2 Additional Laguerre-Gaussian beam on optical lattice

Additional optical trap is required to trap atoms in radial directions. A blue-detuned Laguerre-Gaussian (LG) beam is ideal for spatial confinement in radial directions due to its doughnut-shaped intensity distribution. Combining counter-propagating Gaussian beams and LG beam, atoms can be confined in all directions. The amplitude of the LG_{lp}beam is:

$$u_{lp}(r,\phi,z) = \sqrt{\frac{2p!}{\pi(p+|l|)!}}(\frac{-2r^2}{w^2(z)})^{|l|/2}(L_p^{|l|}(\frac{2r^2}{w^2(z)}))e^{\frac{-r^2}{w^2(z)}}e^{(-i\frac{kr^2z}{2(z^2+z_R^2)}-il\phi+i(2p+l+1)tan^{-1}(\frac{z}{z_R}))} \quad (3.1.3)$$

where $w(z)$ is the beam width, and $L_p^{|l|}$ are are the generalized Laguerre polynomials with mode index l, p. The total intensity of the optical trap is:

$$\begin{aligned} I(\rho,\phi,z) &= |(\frac{2P_1}{\pi w_1^2})^{1/2}\frac{w_1}{w_1(z)}e^{-\frac{\rho^2}{w_1^2(z)}}e^{i[kz+k\frac{\rho^2}{2R_1(z)}-\eta_1(z)]} \\ &- (\frac{2P_2}{\pi w_2^2})^{1/2}\frac{w_2}{w_2(z)}e^{-\frac{\rho^2}{w_2^2(z)}}e^{i[-kz+k\frac{\rho^2}{2R_2(z)}+\eta_2(z)]} \\ &+ \sqrt{\frac{P_3}{w_3^2(z)}}\sqrt{\frac{2p!}{\pi(p+|l|)!}}(\frac{-2r^2}{w^2(z)})^{|l|/2}(L_p^{|l|}(\frac{2r^2}{w^2(z)}))e^{\frac{-r^2}{w^2(z)}}e^{(-i\frac{kr^2z}{2(z^2+z_R^2)}-il\phi+i(2p+l+1)tan^{-1}(\frac{z}{z_R}))}|^2 \end{aligned}$$

where P_3 is the power of the LG beam,$w_3$is the beam waist of the LG beam. LG beam with $l = 1, p = 0$ are used in the following discussion.

doi:10.6342/NTU202201550

3.2 Optical trap properties

3.2.1 Trap properties for ground state atoms

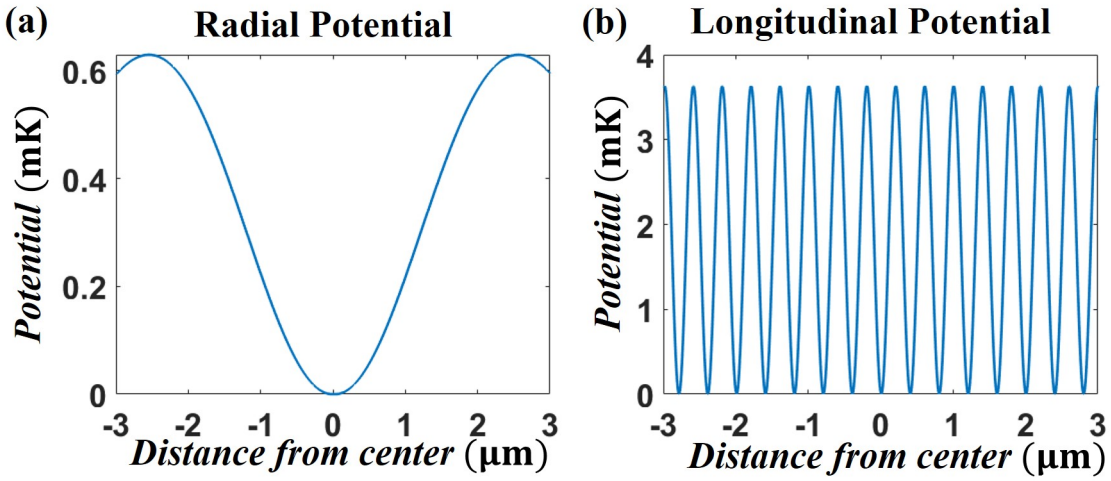

Figure 3.1: The trap depth for ground-state atoms in (a)r-axis provided by the doughnut beam(b) in z-axis relative to the trap center provided by the optical lattice. The horizontal axis is the distance from the center (μm), and the vertical axis is the trap depth (mK).

^{133}Cs and optical lattice with wavelength 780 nm are used in the simulation. The power of the counter-propagating Gaussian beams and the LG beam are $P_1 = P_2 = P_3 = 100$ mW , and the beam waists of the counter-propagating Gaussian beams and the LG beam are $w_1 = w_2 = 5\ \mu$m , $w_3 = 3.6\ \mu$m . Trapping potential for ground-state atoms is represented in Fig.3.1. In the radial directions, as shown in Fig.3.1(a), the trapping potential distribution is similar to the intensity of the LG beam since counter-propagating Gaussian beams are destructive interference at $z = 0$. In the longitudinal direction, as shown in Fig.3.1(b), the potential comes from the counter-propagating Gaussian beams solely since the intensity of the LG beam is 0 at $r = 0$.

doi:10.6342/NTU202201550

3.2.2 Trap properties for Rydberg-state atoms

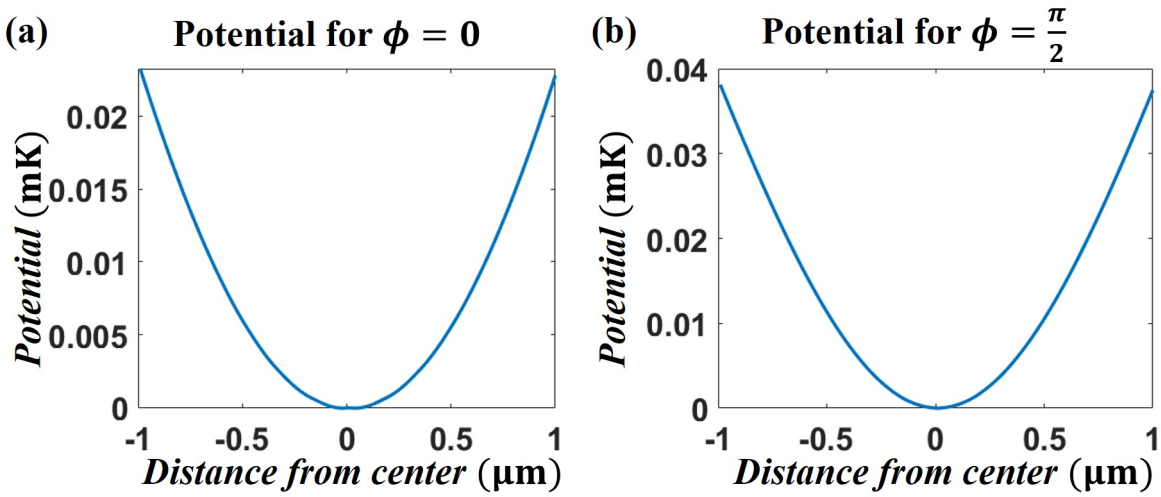

Figure 3.2: The trap depth relative to trap center for Rydberg-state atoms (^{133}Cs in $|100S_{1/2}, m_j = 1/2\rangle$) in r-axis at azimuthal angle (a)$\phi = 0$ (b)$\phi = \frac{\pi}{2}$. The horizontal axis is the distance from the center (μm), and the vertical axis is the trap depth (mK).

The result in Fig.3.2 shows that the trapping potential is much shallower for Rydberg-state atoms in the radial directions. It is because the polarizability for Rydberg-state atoms and ground-state atoms are different. The polarizability of ground-state atom is determined by the wavelength of the optical traps. Yet, the polarizability of Rydberg-state atoms is determined by the ponderomotive force. The trapping potential is different at different azimuthal angles due to the interference between the counter-propagating Gaussian beams and the LG beam. The phase of the Gaussian beam is constant for all azimuthal angles. However, the phase of the LG beam changes with azimuthal angles. Therefore, the optical trap intensity and corresponding potential change with the azimuthal angle.

doi:10.6342/NTU202201550

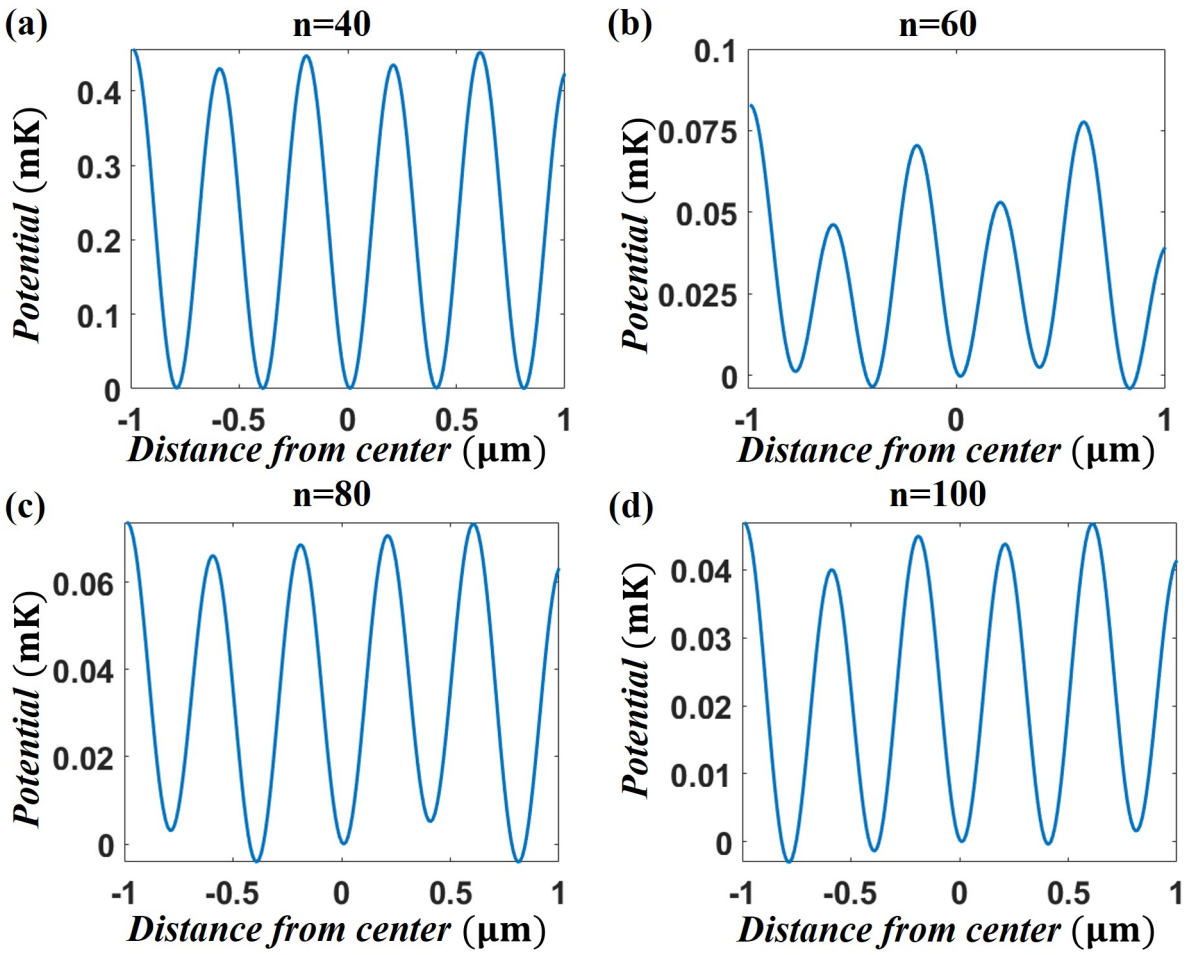

Figure 3.3: The trapping potential relative to trap center for Rydberg-state atoms (^{133}Cs) in longitudinal axis for (a)$|40S_{1/2}, m_j = 1/2\rangle$ (b)$|60S_{1/2}, m_j = 1/2\rangle$ (c)$|80S_{1/2}, m_j = 1/2\rangle$ (d)$|100S_{1/2}, m_j = 1/2\rangle$. The horizontal axis is the distance form the center (μm), and the vertical axis is the trap depth (mK).

The results in Fig.3.3 also demonstrate that the trapping potential is much shallower for Rydberg-state atoms in the longitudinal direction. The ratio of Rydberg-state-to-ground-state trap potential in the longitudinal direction is much smaller than that in the radial direction. Besides the polarizability difference between Rydberg-state atoms and ground-state atoms, the principal quantum number of Rydberg-state atoms also determines the factor [32]. As the results in Fig.3.3(a) to (d), Rydberg-state atom potential varies with principal quantum numbers. For Rydberg-state atoms, the ponderomotive potential is relative to the electronic probability distribution mainly determined by the principal quantum

doi:10.6342/NTU202201550

number. Therefore, sufficient trap depth of atoms in a Rydberg state should be guaranteed for QIP, or additional leakage may occur when atoms are driven to that Rydberg state. Besides, the potential of the Rydberg-state atom is not symmetric to the point at $z = 0$. The non-symmetric potential derives from the interference between the counter-propagating Gaussian beam and the LG beam. The amplitude of the counter-propagating Gaussian beam has roughly π difference for positions at $\pm z$ for arbitrary z near focus on the longitudinal axis. However, the amplitude of LG beam has $2(-\frac{kr^2 z}{2(z^2+z_R^2)} + 2tan^{-1}(\frac{z}{z_R}))$ phase difference for position at $\pm z$ on the longitudinal axis. The intensity of the optical trap, therefore, is not symmetric.

doi:10.6342/NTU202201550

3.3 Quantum gate scheme

Unlike conventional quantum gate implementation on stationary neutral atoms, one of the atoms is moving in the DT scheme (See Fig.3.4). We first assume the velocity of the moving atom is constant (See Fig.3.5). The flying qubit is moving at the beam waist surface of the probing beam.Via engineering, the field intensity and phase are constant on the beam waist surface, so the flying qubit experiences constant field intensity and phase. The probe beam incident on the stationary qubit can be assumed to be constant in field intensity.

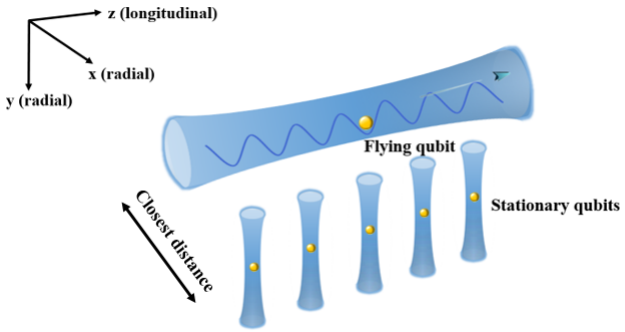

Figure 3.4: The diagram for the Drive-Through method. The flying atom moves via tuning the phase of the optical lattice. The stationary atoms are trapped by blue-detuned optical tweezers.

3.3.1 Rydberg blockade scheme

We first apply the DT method in the Rydberg blockade scheme. As in Fig.3.5, the probe beam is on when the atom is $|\frac{vt}{2}|$ away from the closest point, where t is the gate time $2\pi\Omega^{-1}$, Ω is the Rabi frequency between $|1\rangle$ and the Rydberg state $|r\rangle$. The blockade leakage will be greater since the atoms are more distant during the gate process. Still, the blockade leakage is endurable if $|\frac{vt}{2}|$ is small compared to the closest distance. The result for the Rydberg blockade protocol is shown in Fig.3.6, the closest distance between the two atoms is 10 μm for the Rydberg blockade scheme in the conventional DT scheme. The C_6 coefficient between ^{133}Cs atoms in $|100S_{1/2}, m_j = 1/2\rangle$ is estimated as 4.432×10^4 GHz$\cdot\mu$m^6 , and the interaction energy $V \approx 2\pi\times44.32$ MHz when the distance between the

doi:10.6342/NTU202201550

two atoms is 10 μm and the relative orientation polar angle is 0. The interaction energy varies due to the atom moving is also considered (See Sec.2.1.2). Also, we assume the velocity of the moving atom to be 5 m/s and the Rabi frequency of the probing beam on atoms $\Omega = 2\pi \times 2$ MHz . In the condition, $|\frac{vt}{2}|$ is 2.5 μm , which is small compared to the closet distance. The blockade leakage for the DT method is larger than the conventional method due to the longer initial distance and the final distance between atoms. The corresponding weaker interaction energy causes larger leakage. The blockade leakage is also time-varying due to the time-varying interaction energy.

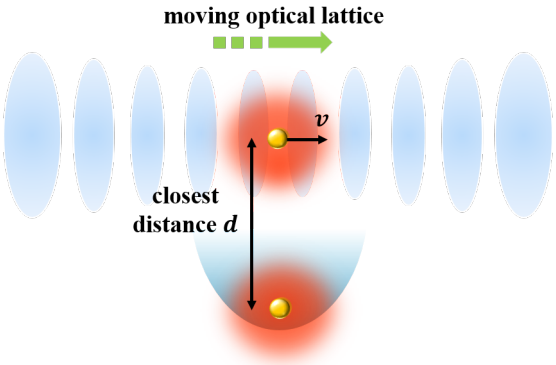

Figure 3.5: The DT method used in QIP. The red areas are the range of the probe beams. We assume the beam intensity and phase are uniform in the probe beam area. Also, the beam waist of the probe beam is larger than $\frac{vt}{2}$, so the flying qubit can interact with the probe beam during the quantum information processing.

3.3.2 Global coupling scheme

We use the DT method on the global coupling scheme [11]. The global coupling scheme relies on different rotation paths on Bloch's sphere for each qubit states. Two qubits are probed by two laser beams with identical phase and intensity simultaneously. The Rabi frequency of single atom coupling to the Rydberg state is Ω, and the couplings of the two atoms to the collective state are different (with a factor of $\sqrt{2}$). An entangling gate can be realized with specifically chosen detuning Δ, single pulse time τ, and relative phase between two pulses ξ. The interaction energy between Rydberg atoms is time-varying in the DT method. Yet, parameters for quantum gate Δ, ξ, τ can still be found to achieve an entangling gate.

doi:10.6342/NTU202201550

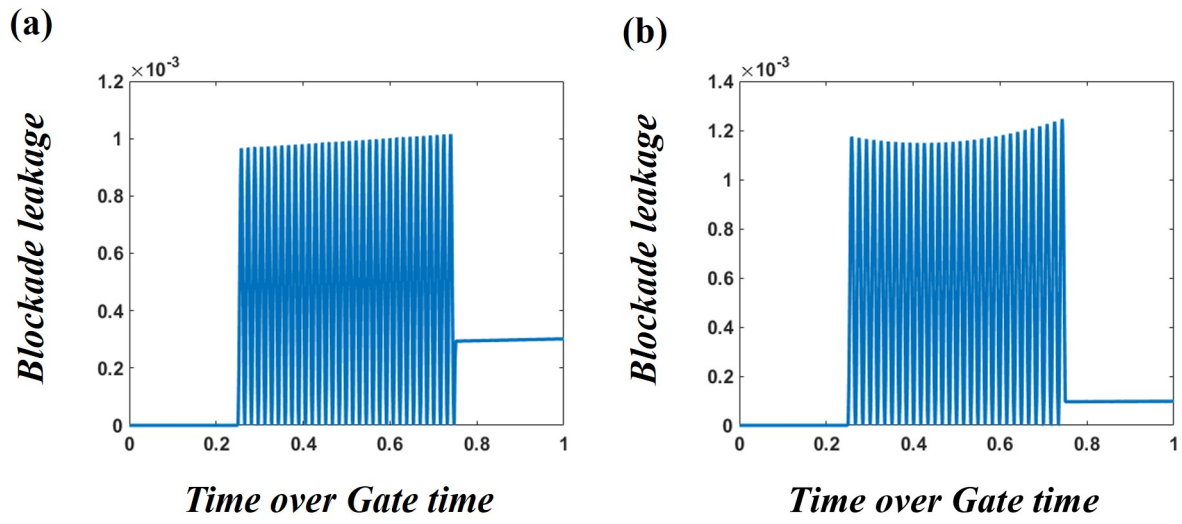

Figure 3.6: The Rydberg blockade protocol for ^{133}Cs atoms in $|100S_{1/2}\rangle$.(a) the Rydberg leakage for Drive-Through method. (b)the Rydberg blockade leakage for two static atoms. The closet distance between two atoms is fixed in 10 μm . The blockade leakage of the scheme is greater than the conventional scheme, and it also varied with time.

In this scheme, $|0\rangle$ does not interact with the probe beam. $\Omega = 2\pi \times 2$ MHz, $\Delta/\Omega = 0.3849, \xi = -2.3726, \tau = \frac{2\pi}{\sqrt{\Delta^2+2\Omega^2}}$, and other parameters are the same as the parameters used in the Rydberg blockade scheme. A two-qubit entangling gate with the global coupling scheme in the DT method with a small error can be accomplished. The result is shown in Fig.3.7. As shown in Fig.3.7(a), the population as well as the states returns after gate implementation for each initial state. Figure.3.7(b) also shows the relative phase $\phi = \phi_{11} - \phi_{01} - \phi_{10}$ is π after evolution. The global coupling scheme works quite well with the DT method.

3.4 Error analysis and gate fidelity

3.4.1 Position fluctuation of atoms in optical traps

Due to the finite optical trap potential, neutral atoms distribute with position distribution when atoms are confined in optical traps. However, a quantum gate can operate ideally only when atoms are in the desired positions. The random distribution in space contributes to errors in the quantum information processing since the interaction energy between

doi:10.6342/NTU202201550

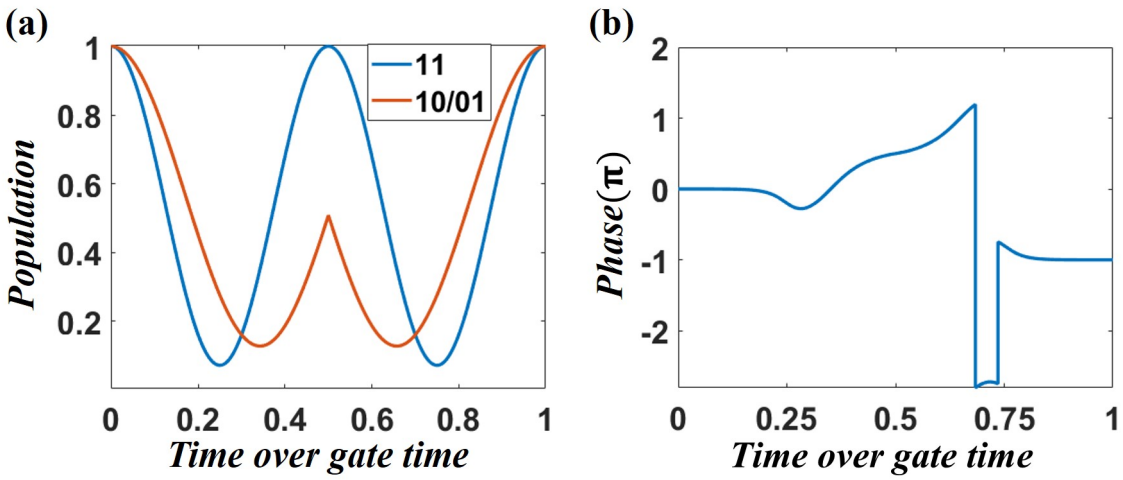

Figure 3.7: The population evolution and accumulated phase of global coupling protocol with the Drive-Through scheme. (a)The evolution of each the initial state. Redline is the population evolution of initial state in $|1\rangle|0\rangle$ or $|0\rangle|1\rangle$ state. Blueline is the population evolution of the initial state in $|1\rangle|1\rangle$ state. (b)The accumulated phase $\phi/\pi = (\phi_{11} - \phi_{01} - \phi_{10})/\pi$ of the entangling gate evolution over time. The phase $\phi/\pi = 1$ after the evolution, as the ideal controlled-Z gate.

Rydberg atoms V is sensitive to their distance. To estimate the spatial distribution, atoms in optical traps are approximated as quantum harmonic oscillators. The assumption is valid when atomic energy is small compared to the trap potential near trap centers because trap potential is still well-approximated to quadratic form in this region.

The distribution of phonon number is determined by the temperature of atoms T and the trap frequency of optical traps ω_i, where index i represents two radial directions and one longitudinal direction. The initial position distribution of atoms in each phonon Fock state follows the wave functions of quantum harmonic oscillators

$$\Psi_n(x_i) = \frac{1}{\sqrt{2^n n!}}\left(\frac{m\omega}{\pi\hbar}\right)^{1/4} e^{-\frac{m\omega x_i^2}{2\hbar}} H_n\left(\sqrt{\frac{m\omega}{\hbar}}x_i\right)$$

where H_n is Hermite polynomials. The phonon number distribution $P(n)$ follows thermal distribution and is proprotional to $e^{-\frac{n\hbar\omega_i}{k_b T}}$. Combining the phonon number distribution and the wave function of each phonon state, the position distribution probability $P(x_i) = \sum_n P_n |\Psi_n(x_i)|^2$.

The trap frequency changes during the quantum gate implementation due to the trap frequency difference between Rydberg-state atoms and ground-state atoms. For atoms in gate implementation, trap frequency $\omega(p_g, p_R) = (p_g\omega_g^2 + p_R\omega_R^2)^{1/2}$, where p_g, p_R is the

doi:10.6342/NTU202201550

probability of atoms in the ground state and Rydberg state respectively. The varying trap frequency ω causes the wave function of the quantum oscillator to expand and contract. Although the wave function expansion will be much slower than the changing of trap frequency, we still assume that the wave functions$\Psi_n(\omega)$ changes with the trap frequency.

The fidelity [See Appendix.A.1] when position fluctuation is considered is shown in Fig.3.8. Both protocols are still robust when the mean phonon number are getting larger because these protocols mainly rely on the blockade from large interaction energy. The interaction energy between Rydberg atoms is still large with position fluctuation.

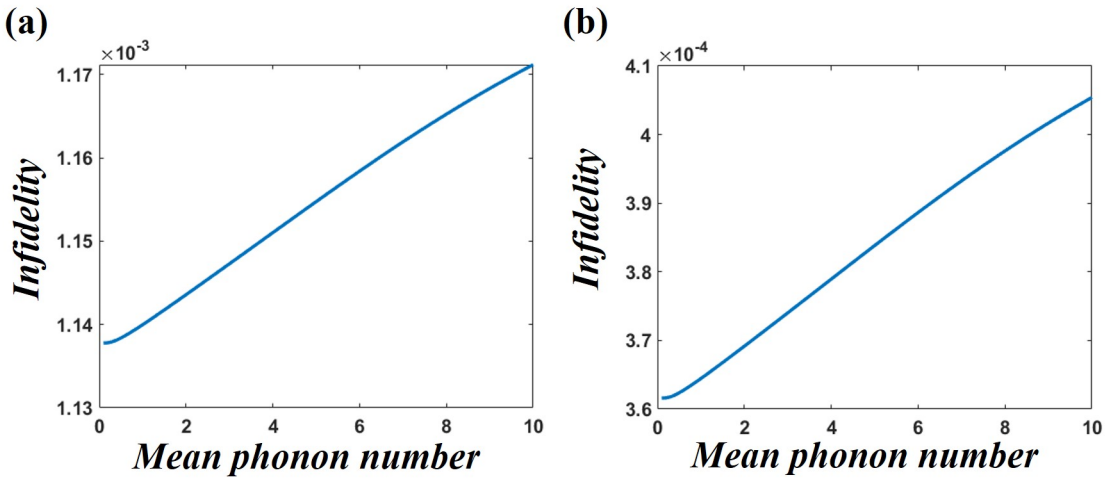

Figure 3.8: (a)The infidelity of the Rydberg blockade scheme when position fluctuation is only considered. (b)The infidelity of the global coupling scheme when position fluctuation is only considered.

3.4.2 Doppler dephasing error

Due to the thermal motion of atoms, atoms get additional Doppler dephasing during the processes of excitations and de-excitations. Doppler dephasing can be eliminated or mitigated in some protocols [33, 34, 35]. However, additional requirements like extra laser pulses and extra time are required. Therefore, incorrectable errors from Doppler dephasing in QIP are directly considered in this work.

In the Rydberg blockade protocol, there are additional phases $e^{ikv_{con,tar}t}$on the controlled qubit and the target qubit, where $v_{con,tar}$ are atomic thermal motions following Maxwell-

doi:10.6342/NTU202201550

Boltzmann distribution.The infidelity is shown in Fig.3.9(a), the random additional phases distribute wider and cause larger errors in higher temperature.

In the global coupling scheme, Doppler dephasing causes random coupling strength between the collective state $\frac{1}{\sqrt{2}}(|1r\rangle + |r1\rangle)$ and the dark state $\frac{1}{\sqrt{2}}(|1r\rangle - |r1\rangle)$. The coupling Rabi frequency $\delta_D \approx 2\pi \frac{v_{con} - v_{tar}}{\lambda}$ results from the difference in the velocities on the controlled qubit and the target qubit. The infidelity is shown in Fig.3.9(b). The fidelity is mainly determined by the ratio of δ_D and Rabi frequency of single atom coupling to Rydberg state Ω. When the temperature is higher, the distribution of δ_D is wider. The corresponding fidelity gets lower.

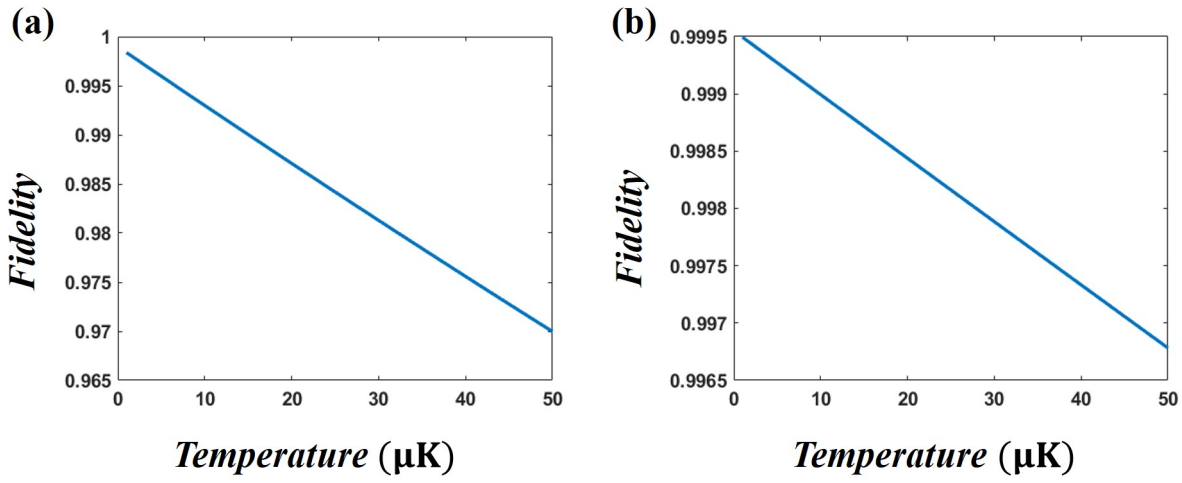

Figure 3.9: The fidelity of (a)the Rydberg blockade protocol (b)the global coupling protocol when doppler effect is only considered.

3.4.3 Spontaneous emission and lifetime factors

Rydberg state decay is one of the main intrinsic errors for quantum information processesing. When atoms are in the Rydberg state, atoms may decay to other states out of calculation basis, thus causing uncorrectable errors. To estimate the decay in QIP, the Lindblad equation is used in numerical simulation. With parameters in Sec.3.3, the gate time $2\tau = 2 \times \frac{2\pi}{\Omega}$ is equal to 1 μs , and the lifetime of an atom in $|100S_{1/2}, m_j = 1/2\rangle$ is 1.062238 ms when atoms are in 10 μK for the Rydberg blockade scheme. The error $\overline{E} = \frac{1}{4}(E_{00} + E_{10} + E_{01} + E_{11})$ is 5.0629×10^{-4}. For global coupling scheme, the gate time

doi:10.6342/NTU202201550

$2\tau = 2\times\frac{2\pi}{\sqrt{\Delta^2+2\Omega^2}}$ is 0.681 μs , and the corresponding error $\overline{E} = 1.9846\times10^{-4}$.

Other factors like scattering rate and photoionization rate [31, 6] play a minor role in the DT method. The scattering rate $\Gamma_{sc}(\vec{r}) = \sum_i \frac{3\pi c^2}{2\hbar\omega_i^3}(\frac{\omega}{\omega_i})^3(\frac{\Gamma}{\omega_i-\omega}+\frac{\Gamma}{\omega_i+\omega})^2 I(\vec{r}) \sim 10\ \mathrm{s}^{-1}$, which is negligible compared to spontaneous emission. On the other hand, the optical lattice strength is in the weak regime, so the Rydberg state is not mixing, and the photoionization rate $\Gamma_{PI} \sim 10\ \mathrm{s}^{-1}$, which is also negligible.

3.4.4 Laser intensity error

The laser intensity error causes the internal states to deviate from ideal results after gate implementation. The result is shown in Fig. 3.10. Both schemes are sensitive to the laser intensity because atomic state evolution is sensitive to the Rabi frequency. When the laser intensity error ratio is to 0.1 (−0.1), the infidelity rises to about 0.05 and 0.035 in each scheme. The Rydberg blockade scheme is more vulnerable because the blockade is incomplete when the controlled-qubit is not exactly in Rydberg state $|r\rangle$. On the contrary, in the global coupling scheme, the double-excited Rydberg states is still blocked when the laser intensity error occurs.

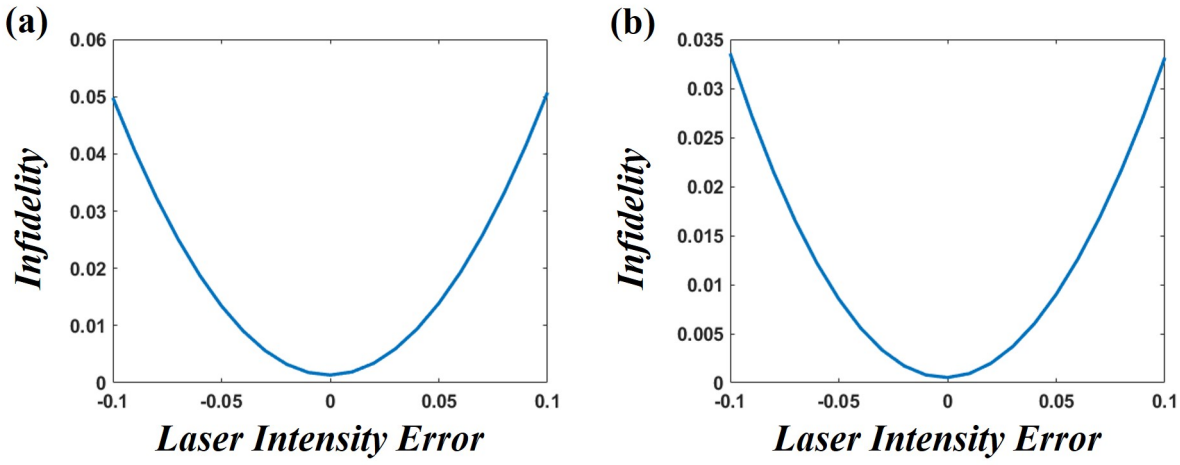

Figure 3.10: The infidelity of (a)the Rydberg blockade scheme (b)the global coupling scheme when probe beam intensity error is only considered. Atoms are assumed in 10 μK .

doi:10.6342/NTU202201550

Chapter 4

Heating effect from acceleration

In this chapter, we will address the main problem in qubit transport, and heating, via engineering the atom trajectories. Phonons are generated and accumulated in the quantum oscillator when atoms are accelerated. Therefore, atoms will eventually escape from the optical trap due to phonon accumulation in repeat transport. To deal with the heating, we aim to avoid phonon generation via engineering the acceleration trajectories. In the remaining of this chapter, we will introduce phonon generation in quantum oscillators from the external force and the scheme to optimize the acceleration process.

4.1 Phonon generation

In the Drive-Through method, an atom is accelerated when the atom departs from its initial position or arrives at its destination. Additional phonons may be generated due to the motion effect, and atoms are more likely to escape from the optical trap. Therefore, preventing heating while transporting atoms is imperative to the Drive-Through method. Before transporting atoms, atoms are assumed to be cooled down in optical traps [36, 37]. The motion state is displaced with $\alpha = \sqrt{\frac{m\omega}{2\hbar}}s(t) - \sqrt{\frac{m\omega}{2\hbar}}(e^{-i\omega t}\int_0^t \dot{s}(t')e^{-i\omega t'}dt')$ [38, 39] at time t, where $s(t)$ is the trap center trajectory. After integration by part, $\alpha = \sqrt{\frac{m\omega}{2\hbar}}s(t) + i\sqrt{\frac{m}{2\hbar\omega}}(\dot{s}(t) - e^{-i\omega t}\int_0^t \ddot{s}(t')e^{-i\omega t'}dt')$. The first term and the second term represent the atomic position shift and velocity shift with the trap center, respectively. The last term

doi:10.6342/NTU202201550

denotes the displacement resulting in heating.

4.2 Acceleration process optimaization

By engineering the time-dependent acceleration $\ddot{s}(t)$, desired final velocity v and low phonon generation during the process can be attained with the condition that

$$\int_0^{t_f} \ddot{s}(t)dt = \dot{s}(t_f) = \pm v \tag{4.2.1}$$

and

$$\left|\int_0^{t_f} a(t)e^{-i\omega_0 t}dt\right| \leq \epsilon \tag{4.2.2}$$

where t_f is the end time of acceleration, and ϵ is a given standard that makes sure the generated phonon number ΔN sufficient low.

doi:10.6342/NTU202201550

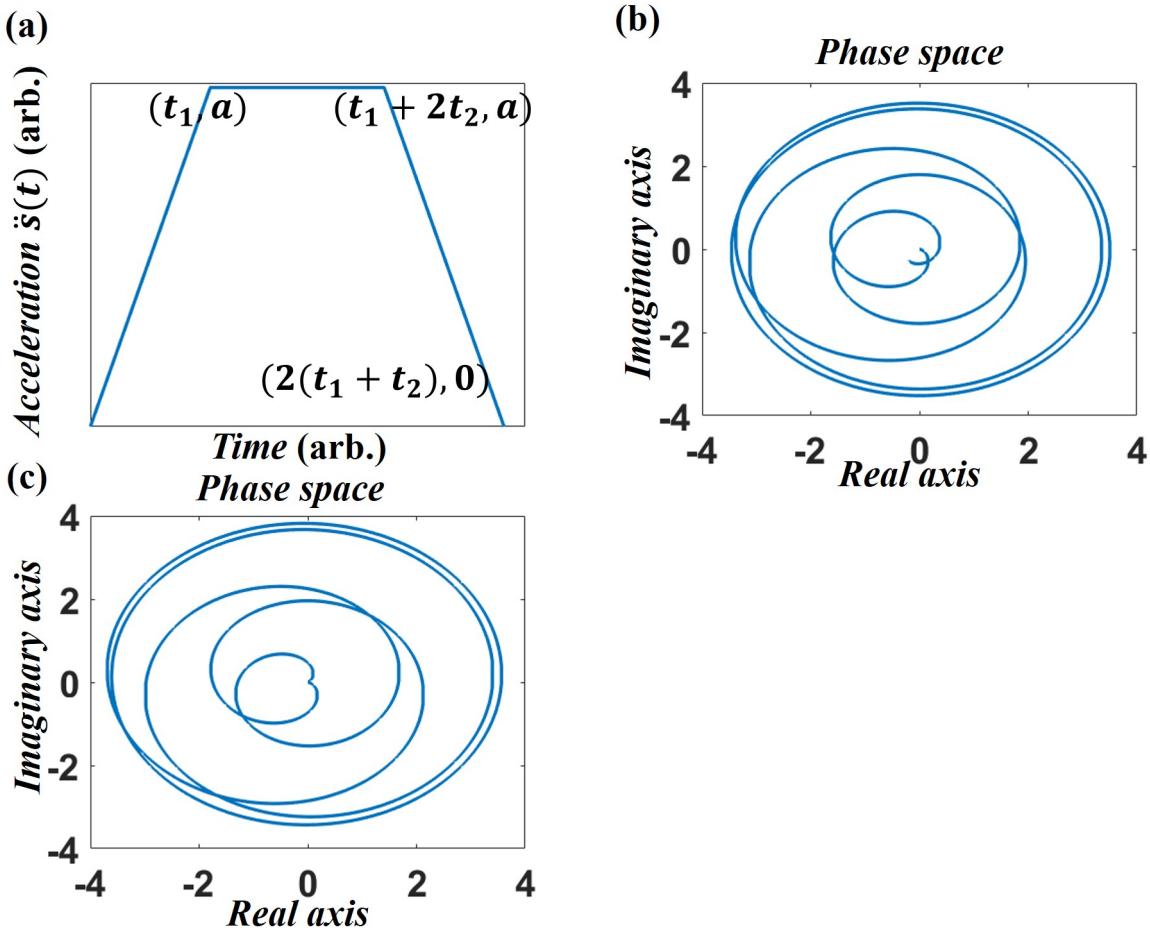

Figure 4.1: (a)The scheme of acceleration $a(t)$ changes over time. (b)The phase space of the harmonic oscillator during the acceleration process with original parameters. (c)The phase space of the harmonic oscillator during the acceleration process with tuned parameters.

We assume that the acceleration process is as followed: as Fig.4.1(a), when $t = 0$ to $t = t_1$, the acceleration linear increases from 0 to a. When $t = t_1$ to $t = t_1 + 2t_2$, the acceleration keeps as a. When $t = t_1 + 2t_2$ to $t = 2(t_1 + t_2)$, the acceleration linear decreases from a to 0. Following the condition above and set $\epsilon = 0$, we have:

$$a(\frac{t_1}{2} + t_2) = \frac{v}{2} \tag{4.2.3}$$

doi:10.6342/NTU202201550

and

$$|\int_0^{t_f} \ddot{s}(t)e^{-i\omega_0 t}dt| = \frac{2a}{\omega_0^2 t_1}|(cos(\omega_0(t_1+t_2)) - cos(\omega_0 t_2))| = 0 \quad (4.2.4)$$

. Therefore, $t_1 = n(\frac{2\pi}{\omega_0})$. There is still some flexibility for choosing a and t_2.

In the Drive-Through method, the longitudinal trap frequency for ground-state atoms $\omega_0 = 2\pi \times 693.116$ kHz when atoms are roughly 47 μm away from the focus. $t_1 = 2 \times \frac{2\pi}{\omega_0} = 2.886$ μs . $t_2 = 1\mu$s . Then $a = 1.0233 \times 10^6$ m/s^2 are chosen for numerical simulation. The total distance atoms move in the acceleration process is 20.851 μm , which is short for the Rayleigh range of the optical lattice.

However, the trap frequency is varied with the distance from the center because the beam waist and laser intensity vary with the distance from the focus. Mean phonon number changes $\Delta N = |\alpha|^2 = 0.1139$ when the effect is included. The result is plotted in Fig.4.1(b). The mean phonon number change ΔN is still small. Since the trap frequency changed during the transportation is mild, new parameters can be found near the original parameters to further lower phonons generated from the acceleration. When $a = 1.0571 \times 10^6$m/s^2 , $t_1 = 2.73\mu$s , $t_2 = 1$ μs, mean phonon number changes ΔN lower than 10^{-4}. Fig.4.1(c) shows the motion state evolves close to the original state. Low change phonon number represents that the heating effect from the acceleration process is almost negligible. Also, $\Delta N(t) \ll$ trap depth when $t < t_f$ also promises the atomic confinement in the process.

doi:10.6342/NTU202201550

Chapter 5

Conclusion

In summary, we present the design of optical traps for the Drive-Through method. Both ground-state atoms and Rydberg-state atoms can be trapped using blue-detuned optical lattices and a Laguerre-Gaussian beam. Trapping potential for ground-state atoms and Rydberg-state atoms is also represented in Sec.3. An optical trap with deep trap depth for both ground-state atoms and Rydberg-state atoms promises the atomic confinement during the gate implementation. Besides, the results in Sec.3 demonstrate two-qubit entangling gates can be realized with high fidelity in the Rydberg blockade scheme and the global coupling scheme. It shows the viability of simultaneous atomic transport and high fidelity quantum information processing, and a potential solution to the connectivity in neutral atom systems for quantum information processing.

One advantage of using a counter-propagating Gaussian beam in the Drive-Through method is that atoms can move smoothly, so atoms do not need to be accelerated frequently while transporting. Heating from the movement only derives from acceleration at the start point and deceleration at the destination. In Sec.4, we show that the phonon generation from acceleration can be eliminated via engineering the moving trajectories. Therefore, atoms are robust to the heating from the transport. The other advantage is that atoms can be accelerated to high speed without loss instantly due to the deep trap depth. The high speed results in a shorter transportation time, so dephasing effect and decoherence from other experimental sources will not dominate during the transport.

doi:10.6342/NTU202201550

The error sources are shown in Sec.3.4. One comes from the atomic spatial distribution in optical traps. Although Rydberg-state atoms are confined with lower trap frequency, the errors from random spatial distribution are still small enough. As for the inevitable error source, Rydberg decay, one can mitigate the decay by choosing a Rydberg state with a longer lifetime or using a stronger probing beam to shorter the gate time. The Stark shift from the trapping laser is not discussed in this work. Since atoms are trapped in space with a weak laser intensity of blue-detuned optical lattice, the Stark shift from trapping laser should be experimental amendable. Still, we leave these improvable factors as future works.

doi:10.6342/NTU202201550

doi:10.6342/NTU202201550

doi:10.6342/NTU202201550

Appendix A

Derivation

A.1 Average fidelity

A.1.1 Fidelity

The fidelity is defined by the Bell's state preparation. The fidelity $F \equiv (Tr_Q\sqrt{(\sqrt{\rho}\rho_{id}\sqrt{\rho})})^2$ [40], where ρ_{id} denotes the ideal density matrix of Bell's state $|\Phi^+\rangle\langle\Phi^+|$, and $|\Phi^+\rangle = \frac{1}{\sqrt{2}}(|00\rangle+|11\rangle)$. Q denotes the calculation basis$|00\rangle, |01\rangle|11\rangle, |11\rangle$. ρ is the density matrix of $U(\tau)|\Psi(0)\rangle$, where $|\Psi(0)\rangle = \frac{1}{\sqrt{2}}(|0\rangle+|1\rangle)|0\rangle$, $U(\tau) = (I \bigotimes R(\pi, \tilde{\phi}, -\tilde{\phi}, 0))U_{cz,\phi}(I \bigotimes R(0,0,0,\pi)),\tau$ is the time of gate operation, $U_{cz,\phi}$represents the operator of the gate implementation, and $\tilde{\phi}$ denotes the phase difference between final states initially in $|10\rangle$ and $|11\rangle$. $R(\overrightarrow{h}) = \frac{1}{\sqrt{2}}\begin{pmatrix} e^{ih_{00}} & e^{ih_{01}} \\ e^{ih_{10}} & e^{ih_{11}} \end{pmatrix}$, where $\overrightarrow{h} = \begin{pmatrix} h_{00} & h_{01} & h_{10} & h_{11} \end{pmatrix}$. If the entangling phase $\phi_{00} - \phi_{01} - \phi_{10} + \phi_{11}$is ideally π and the state can be spanned by the basis Q, then $U(\tau) = (I \bigotimes R(\pi, \tilde{\phi}, -\tilde{\phi}, 0))U_{cz,\phi}(I \bigotimes R(0,0,0,\pi))$ produces the ideal CNOT-gate.

A.1.2 Average fidelity over atomic positions

The average fidelity function is defined as $\overline{\mathcal{F}} = \int D(\overrightarrow{r}_{flying}, \overrightarrow{r}_{stationary})d^6r\mathcal{F}$, where $\mathcal{F}$ is the fidelity of the quantum operation at the specific atomic position $\overrightarrow{r}_{flying}$ and $\overrightarrow{r}_{static}$

doi:10.6342/NTU202201550

relative to their trap centers. The fidelity is defined by Bell's state preparation. D is the probability distribution of atomic positions.

A.1.3 Average fidelity over atomic doppler velocity

Similarly, the average fidelity function is defined as $\overline{\mathcal{F}} = \int D(\overrightarrow{v}_{flying}, \overrightarrow{v}_{stationary}) d^3 r \mathcal{F}$, where $\mathcal{F}$ is the fidelity of the quantum operation with specific atomic velocity $\overrightarrow{v}_{drive}$ and $\overrightarrow{v}_{stationary}$. The fidelity is defined by Bell's state preparation. D is the probability distribution of atomic velocities.

doi:10.6342/NTU202201550

Bibliography

[1] M. Saffman and T. G. Walker. Analysis of a quantum logic device based on dipole-dipole interactions of optically trapped rydberg atoms. *Physical Review A*, 72(2):022347, aug 2005.

[2] Thad G. Walker and M. Saffman. Consequences of zeeman degeneracy for the van der waals blockade between rydberg atoms. *Physical Review A*, 77(3):032723, mar 2008.

[3] M. Saffman, T. G. Walker, and K. Mølmer. Quantum information with rydberg atoms. *Reviews of Modern Physics*, 82(3):2313–2363, aug 2010.

[4] M Saffman. Quantum computing with atomic qubits and rydberg interactions: progress and challenges. *Journal of Physics B: Atomic, Molecular and Optical Physics*, 49(20):202001, oct 2016.

[5] J. T. Wilson, S. Saskin, Y. Meng, S. Ma, R. Dilip, A. P. Burgers, and J. D. Thompson. Trapping alkaline earth rydberg atoms optical tweezer arrays. *Physical Review Letters*, 128(3):033201, jan 2022.

[6] S. Zhang, F. Robicheaux, and M. Saffman. Magic-wavelength optical traps for rydberg atoms. *Physical Review A*, 84(4):043408, oct 2011.

[7] Sepehr Ebadi, Tout T. Wang, Harry Levine, Alexander Keesling, Giulia Semeghini, Ahmed Omran, Dolev Bluvstein, Rhine Samajdar, Hannes Pichler, Wen Wei Ho, Soonwon Choi, Subir Sachdev, Markus Greiner, Vladan Vuletić, and Mikhail D.

doi:10.6342/NTU202201550

Lukin. Quantum phases of matter on a 256-atom programmable quantum simulator. *Nature*, 595(7866):227–232, jul 2021.

[8] F. M. Gambetta, W. Li, F. Schmidt-Kaler, and I. Lesanovsky. Engineering NonBinary rydberg interactions via phonons in an optical lattice. *Physical Review Letters*, 124(4):043402, jan 2020.

[9] H. Schempp, G. GÃijnter, S. WÃijster, M. WeidemÃijller, and S. Whitlock. Correlated exciton transport in rydberg-dressed-atom spin chains. *Physical Review Letters*, 115(9):093002, aug 2015.

[10] Johannes Zeiher, Jae yoon Choi, Antonio Rubio-Abadal, Thomas Pohl, Rick van Bijnen, Immanuel Bloch, and Christian Gross. Coherent many-body spin dynamics in a long-range interacting ising chain. *Physical Review X*, 7(4):041063, dec 2017.

[11] Harry Levine, Alexander Keesling, Giulia Semeghini, Ahmed Omran, Tout T. Wang, Sepehr Ebadi, Hannes Bernien, Markus Greiner, Vladan Vuletić, Hannes Pichler, and Mikhail D. Lukin. Parallel implementation of high-fidelity multiqubit gates with neutral atoms. *Phys. Rev. Lett.*, 123:170503, Oct 2019.

[12] T. M. Graham, M. Kwon, B. Grinkemeyer, Z. Marra, X. Jiang, M. T. Lichtman, Y. Sun, M. Ebert, and M. Saffman. Rydberg-mediated entanglement in a two-dimensional neutral atom qubit array. *Physical Review Letters*, 123(23):230501, dec 2019.

[13] Ivaylo S. Madjarov, Jacob P. Covey, Adam L. Shaw, Joonhee Choi, Anant Kale, Alexandre Cooper, Hannes Pichler, Vladimir Schkolnik, Jason R. Williams, and Manuel Endres. High-fidelity entanglement and detection of alkaline-earth rydberg atoms. *Nature Physics*, 16(8):857–861, may 2020.

[14] T. M. Graham, Y. Song, J. Scott, C. Poole, L. Phuttitarn, K. Jooya, P. Eichler, X. Jiang, A. Marra, B. Grinkemeyer, M. Kwon, M. Ebert, J. Cherek, M. T. Lichtman, M. Gillette, J. Gilbert, D. Bowman, T. Ballance, C. Campbell, E. D. Dahl, O. Crawford, N. S. Blunt, B. Rogers, T. Noel, and M. Saffman. Multi-qubit entanglement

doi:10.6342/NTU202201550

and algorithms on a neutral-atom quantum computer. *Nature*, 604(7906):457–462, apr 2022.

[15] Antoine Browaeys, Daniel Barredo, and Thierry Lahaye. Experimental investigations of dipole–dipole interactions between a few rydberg atoms. *Journal of Physics B: Atomic, Molecular and Optical Physics*, 49(15):152001, jun 2016.

[16] E. Urban, T. A. Johnson, T. Henage, L. Isenhower, D. D. Yavuz, T. G. Walker, and M. Saffman. Observation of rydberg blockade between two atoms. *Nature Physics*, 5(2):110–114, jan 2009.

[17] Alpha GaÃńtan, Yevhen Miroshnychenko, Tatjana Wilk, Amodsen Chotia, Matthieu Viteau, Daniel Comparat, Pierre Pillet, Antoine Browaeys, and Philippe Grangier. Observation of collective excitation of two individual atoms in the rydberg blockade regime. *Nature Physics*, 5(2):115–118, jan 2009.

[18] D. Barredo, S. Ravets, H. Labuhn, L. Béguin, A. Vernier, F. Nogrette, T. Lahaye, and A. Browaeys. Demonstration of a strong rydberg blockade in three-atom systems with anisotropic interactions. *Physical Review Letters*, 112(18):183002, may 2014.

[19] Alexey V. Gorshkov, Johannes Otterbach, Michael Fleischhauer, Thomas Pohl, and Mikhail D. Lukin. Photon-photon interactions via rydberg blockade. *Physical Review Letters*, 107(13):133602, sep 2011.

[20] Daniel Tiarks, Steffen Schmidt-Eberle, Thomas Stolz, Gerhard Rempe, and Stephan DÃijrr. A photon–photon quantum gate based on rydberg interactions. *Nature Physics*, 15(2):124–126, oct 2018.

[21] X. X. Li, J. B. You, X. Q. Shao, and Weibin Li. Coherent ground-state transport of neutral atoms. *Physical Review A*, 105(3):032417, mar 2022.

[22] V. Subrahmanyam. Entanglement dynamics and quantum-state transport in spin chains. *Physical Review A*, 69(3):034304, mar 2004.

doi:10.6342/NTU202201550

[23] Dolev Bluvstein, Harry Levine, Giulia Semeghini, Tout T. Wang, Sepehr Ebadi, Marcin Kalinowski, Alexander Keesling, Nishad Maskara, Hannes Pichler, Markus Greiner, Vladan Vuletic, and Mikhail D. Lukin. A quantum processor based on coherent transport of entangled atom arrays, 2021.

[24] Ryan Cardman and Georg Raithel. Circularizing rydberg atoms with time-dependent optical traps. *Physical Review A*, 101(1):013434, jan 2020.

[25] Cheng Sheng, Xiaodong He, Peng Xu, Ruijun Guo, Kunpeng Wang, Zongyuan Xiong, Min Liu, Jin Wang, and Mingsheng Zhan. High-fidelity single-qubit gates on neutral atoms in a two-dimensional magic-intensity optical dipole trap array. *Physical Review Letters*, 121(24):240501, dec 2018.

[26] Thomas F. Gallagher. *Rydberg Atoms*. Cambridge University Press, sep 1994.

[27] G. T. Hickman and M. Saffman. Speed, retention loss, and motional heating of atoms in an optical conveyor belt. *Physical Review A*, 101(6):063411, jun 2020.

[28] T. Xia, M. Lichtman, K. Maller, A. W. Carr, M. J. Piotrowicz, L. Isenhower, and M. Saffman. Randomized benchmarking of single-qubit gates in a 2d array of neutral-atom qubits. *Physical Review Letters*, 114(10):100503, mar 2015.

[29] M. J. Piotrowicz, M. Lichtman, K. Maller, G. Li, S. Zhang, L. Isenhower, and M. Saffman. Two-dimensional lattice of blue-detuned atom traps using a projected gaussian beam array. *Physical Review A*, 88(1):013420, jul 2013.

[30] S. K. Dutta, J. R. Guest, D. Feldbaum, A. Walz-Flannigan, and G. Raithel. Ponderomotive optical lattice for rydberg atoms. *Physical Review Letters*, 85(26):5551–5554, dec 2000.

[31] R Cardman, J L MacLennan, S E Anderson, Y-J Chen, and G Raithel. Photoionization of rydberg atoms in optical lattices. *New Journal of Physics*, 23(6):063074, jun 2021.

doi:10.6342/NTU202201550

[32] K. C. Younge, B. Knuffman, S. E. Anderson, and G. Raithel. State-dependent energy shifts of rydberg atoms in a ponderomotive optical lattice. *Physical Review Letters*, 104(17):173001, apr 2010.

[33] I. I. Ryabtsev, I. I. Beterov, D. B. Tretyakov, V. M. Entin, and E. A. Yakshina. Doppler- and recoil-free laser excitation of rydberg states via three-photon transitions. *Physical Review A*, 84(5):053409, nov 2011.

[34] Xiao-Feng Shi. Suppressing motional dephasing of ground-rydberg transition for high-fidelity quantum control with neutral atoms. *Physical Review Applied*, 13(2):024008, feb 2020.

[35] Tyler Keating, Robert L. Cook, Aaron M. Hankin, Yuan-Yu Jau, Grant W. Biedermann, and Ivan H. Deutsch. Robust quantum logic in neutral atoms via adiabatic rydberg dressing. *Physical Review A*, 91(1):012337, jan 2015.

[36] A. M. Kaufman, B. J. Lester, and C. A. Regal. Cooling a single atom in an optical tweezer to its quantum ground state. *Physical Review X*, 2(4):041014, nov 2012.

[37] J. D. Thompson, T. G. Tiecke, A. S. Zibrov, V. Vuletić, and M. D. Lukin. Coherence and raman sideband cooling of a single atom in an optical tweezer. *Physical Review Letters*, 110(13):133001, mar 2013.

[38] R. Reichle, D. Leibfried, R.B. Blakestad, J. Britton, J.D. Jost, E. Knill, C. Langer, R. Ozeri, S. Seidelin, and D.J. Wineland. Transport dynamics of single ions in segmented microstructured paul trap arrays. *Fortschritte der Physik*, 54(8-10):666–685, aug 2006.

[39] Hoi-Kwan Lau and Daniel F. V. James. Decoherence and dephasing errors caused by the dc stark effect in rapid ion transport. *Physical Review A*, 83(6):062330, jun 2011.

[40] L. S. Theis, F. Motzoi, F. K. Wilhelm, and M. Saffman. High-fidelity rydberg-blockade entangling gate using shaped, analytic pulses. *Physical Review A*, 94(3):032306, sep 2016.

doi:10.6342/NTU202201550

doi:10.6342/NTU202201550